Research Article

Muhammad Ramzan, Abdullah Dawar, Anwar Saeed*, Poom Kumam*, Kanokwan Sitthithakerngkiet, and Showkat Ahmad Lone

Analysis of the partially ionized kerosene oil-based ternary nanofluid flow over a convectively heated rotating surface

https://doi.org/10.1515/phys-2022-0055
received April 29, 2022; accepted June 05, 2022

Abstract: The main goal of this inspection is to explore the heat and mass transport phenomena of a three-dimensional magnetohydrodynamic (MHD) flow of ternary hybrid nanoliquid through a porous media toward a stretching surface. Nowadays, the low thermal conductivity is the key problem for scientist and researchers in the transmission of heat processes. Therefore, in order to improve the thermal conductivity of different base liquids, the scientist and researchers are mixing numerous types of solid particles in the base fluids. That is why the authors have mixed three different types of nanoparticles such as graphene oxide, silver, and copper in a kerosene oil base liquid. The influences of Hall current and ion-slip are also considered. Furthermore, the flow behavior is analyzed under the appliance of Darcy–Forchheimer, activation energy, and chemical reaction. By using the concept of boundary layer theory, the flow equations are modeled in the form of higher order nonlinear partial differential equations (PDEs) along with convective boundary conditions. Suitable similarity transformations are used for the transformation of higher order PDEs into the higher order nonlinear ordinary differential equations (ODEs). Analytical scheme known as the homotopic scheme is utilized for the simulation of the current problem. The impacts of discrete flow parameters on the velocities, temperature, and concentration profiles of the ternary hybrid nanoliquid are inspected. The skin friction coefficients, Nusselt number, and Sherwood number of the ternary hybrid nanofluid are investigated against various flow parameters. The outcomes of the current analysis showed that primary velocity of the ternary hybrid nanoliquid is augmented *via* Hall current and ion-slip number, while the reverse trend is observed *via* porosity parameter, Darcy–Forchheimer parameter, and magnetic field parameter. On the other hand, the higher values of Hall current and magnetic parameter enhanced the secondary velocity of the ternary hybrid nanoliquid, while the secondary velocity was reduced due to the increasing ion-slip number and rotation parameter. It is found that the heat transfer rate of the ternary hybrid nanofluid is 46% greater than the silver nanofluid.

*** Corresponding author: Anwar Saeed,** Department of Mathematics, Center of Excellence in Theoretical and Computational Science (TaCS-CoE), Science Laboratory Building, Faculty of Science, King Mongkut's University of Technology Thonburi (KMUTT), 126 Pracha-Uthit Road, Bang Mod, Thung Khru, Bangkok 10140, Thailand, e-mail: anwarsaeed769@gmail.com
*** Corresponding author: Poom Kumam,** KMUTT Fixed Point Research Laboratory, Room SCL 802 Fixed Point Laboratory, Science Laboratory Building, Department of Mathematics, Faculty of Science, King Mongkut's University of Technology Thonburi (KMUTT), Bangkok 10140, Thailand; Department of Mathematics, Center of Excellence in Theoretical and Computational Science (TaCS-CoE), Science Laboratory Building, Faculty of Science, King Mongkut's University of Technology Thonburi (KMUTT), 126 Pracha-Uthit Road, Bang Mod, Thung Khru, Bangkok 10140, Thailand; Department of Medical Research, China Medical University Hospital, China Medical University, Taichung 40402, Taiwan, e-mail: poom.kum@kmutt.ac.th
Muhammad Ramzan: KMUTT Fixed Point Research Laboratory, Room SCL 802 Fixed Point Laboratory, Science Laboratory Building, Department of Mathematics, Faculty of Science, King Mongkut's University of Technology Thonburi (KMUTT), Bangkok 10140, Thailand; Department of Mathematics, Center of Excellence in Theoretical and Computational Science (TaCS-CoE), Science Laboratory Building, Faculty of Science, King Mongkut's University of Technology Thonburi (KMUTT), 126 Pracha-Uthit Road, Bang Mod, Thung Khru, Bangkok 10140, Thailand
Abdullah Dawar: Department of Mathematics, Abdul Wali Khan University Mardan, Mardan, 23200, Khyber Pakhtunkhwa, Pakistan
Kanokwan Sitthithakerngkiet: Intelligent and Nonlinear Dynamic Innovations Research Center, Department of Mathematics, Faculty of Applied Science, King Mongkut's University of Technology North Bangkok (KMUTNB), 1518, Wongsawang, Bangsue, Bangkok 10800, Thailand
Showkat Ahmad Lone: Department of Basic Sciences, College of Science and Theoretical Studies, Saudi Electronic University, Jeddah-M, Riyadh 11673, Saudi Arabia

Keywords: MHD flow, ternary nanofluid, nanoparticles, kerosene oil, Hall current, rotating surface

Nomenclature

A and B	constants
B_0	strength of magnetic field
$\mathrm{Bi_T}$	thermal Biot number
$\mathrm{Bi_C}$	solutal Biot number
$\bar{C}$	concentration
$\bar{C}_w$	surface concentration
$\bar{C}_\infty$	ambient concentration
C_p	specific heat
C_x and C_y	skin friction coefficients
D_B	Brownian diffusion coefficient
E	dimensionless activation energy
E_a	dimensional activation energy
Ec	Eckert number
Fr	Darcy-Forchheimer
F_s	coefficient of inertia
$k^\star$	permeability of the porous media
k	thermal conductivity
k_c	chemical reaction rate
kr	chemical reaction parameter
M	magnetic field
n	power index
Nu	Nusselt number
Pr	Prandtl number
Re_x, Re_y	Reynolds number
Sc	Schmidt number
Sh	Sherwood number
$\bar{T}$	nanofluid temperature
$\bar{T}_w$	surface temperature
$\bar{T}_\infty$	ambient temperature
$\bar{u}$, $\bar{v}$, $\bar{w}$	velocity components
ν	kinematic viscosity
ρ	density
γ_e	Hall current
γ_i	ion-slip number
σ	electrical conductivity
ξ	similarity variable
Ω	rotation parameter
ε	porosity parameter
ϕ	volume fraction of the nanoparticles

1 Introduction

Several researchers have recently become interested in the wide range of applications of nanoliquid in manufacturing, medical, and other domains. From the concept of the nanoliquid, it is observed that the nanoliquid is a mixture of the nanoparticles and base liquid. Aluminum oxide, copper (Cu), silver (Ag), graphene, and many others are some of the nanoparticles. In the literature, different studies on the nanofluids explained that the nanofluids have a superior capability of heat transport as compared to the regular liquids. The heat transport capability of the working fluid is improved by the suspensions of nanoparticles in a base liquid, that is why the thermophysical properties of the fluid are enhanced. The nanofluid is very useful in cooling systems, heat generators, heat exchangers, fuel cells, hybrid powered engines, microelectronics, domestic refrigerators, grinding machines, pharmaceutical procedures, *etc*. As a result, mathematicians and researchers are concerned with studying nanofluid phenomena to enhance the thermal performance of the base liquids. Farooq *et al.* [1] discussed the presence of Cattaneo–Christov heat flux for the improvement of heat transportation over the melting flow of nanoliquid under extending surface. In this investigation, it is evaluated that the rising estimation of the melting parameter reduced the nanoliquid temperature. Li *et al.* [2] deliberated the role of a chemical reaction and mass transmission over the magnetohydrodynamic (MHD) flow of nanoliquid above the vertical plate. For the numerical computation, they utilized the bvp4c technique in the modeling of their study. Sunthrayuth *et al.* [3] expounded on the phenomena of homogeneous–heterogeneous chemical reaction over the flow of second-grade nanoliquid under the melting surface. Ramzan *et al.* [4] checked the existence of motile gyrotactic microorganism and activation energy on the non-Newtonian second-grade nanoliquid flow induced by the thin needle. In this area of work, they found that the motile density of the nanofluid declined due to the change in bioconvection Lewis number. Ramzan *et al.* [5] explicated the presence of Hall current and magnetic field on the two-dimensional flow of nanoliquid under the spinning disk by using the von Karman similarity transformations. In this examination, they used water as a base liquid and gold (Au), silver (Ag), and silicon

dioxide (SiO_2) are the nanoparticles. Gul *et al.* [6] inspected the occurrence of Darcy–Forchheimer over the flow of hybrid nanoliquid in the presence of viscous dissipation toward the moving thin needle. Ramzan *et al.* [7] made the mathematical modeling of the Burger nanofluid with thermal and zero mass flux conditions by using the homotopic scheme in a stretching cylinder. In this inspection, they computed that the thermal Biot number raised the Nusselt number (Nu) of the nanofluid. Alghamdi *et al.* [8] highlighted the features of the thermal radiation and heat transport on the mixed convection flow of Casson nanoliquid with the magnetic effect by using the Darcy–Brinkman porous medium toward the slender surface. Rasool and Wakif [9] used the convective boundary conditions for the computation of the Cattaneo–Christov heat flux on the mixed flow of second-grade nanoliquid under the vertical Riga plate. In this evaluation, it is predicted that with the expanding of the second-grade liquid parameter, the velocity of the nanoliquid is diminished. Ashraf *et al.* [10] implemented the generalized differential quadrature technique for the numerical solution of the MHD peristaltic blood-based Casson nanoliquid flow toward the uniform tube. Mjankwi *et al.* [11] presented the impact of the chemical reaction on the flow of nanoliquid with magnetic field and variable properties past a stretching surface. In this work, it is detected that the nanoliquid temperature is increased with the upsurge in the thermal conductivity of the nanofluid. Wakif *et al.* [12] analyzed the role of the Joule heating and wall suction impacts over the flow of nanoliquid under the moving horizontal Riga plate and examined that rate of the heat transport is enhanced due to the increase in the wall suction parameter. Further studies related to the nanofluid flow problems under different geometries can be cited as refs [13–15].

The thermal performance of the base liquid is improved by adding the single nanoparticle in a single base liquid but it does not show more satisfactory results in the improvement of the thermal performance of the base liquid. To overcome this problem, two distinct kinds of nanoparticles are mixed up to a single base liquid known as the hybrid nanoliquid which showed more satisfactory results for the improvement of thermal performance of the base fluid as compared to the nanoliquid and regular fluid. Hybrid nanoliquids have a lot of applications in different types of engineering and industrial field. Some significant applications of the hybrid nanofluid are nuclear industries, exotic lubricant, paper manufacture, chemical industries, polymer solution geophysical processes, transportations, suspension and colloidal solution, clinical climbing, microfluidics, biomedical applications, heat pipes, cooling of the electronic components, machining, solar thermal systems, heat exchangers, *etc*. Different scientists and researchers adopted hybrid nanofluid in their areas of research due to the abovementioned applications. Khan *et al.* [16] offered the flow analysis of the MoS_2–GO hybrid nanofluid through the porous media under the slender revolution bodies with thermal radiation and discussed that the slender body parameter upsurges the velocity of the hybrid nanoliquid. Khan *et al.* [17] considered the occurrence of Darcy–Forchheimer in the simulation of time-dependent electroviscous and hybrid nanoliquid flow between the two squeezing plates and employed the homotopy analysis procedure for the analytical simulation of their problem. Gumber *et al.* [18] deliberated the behavior of suction/injection over the flow of micropolar hybrid nanoliquid on the incidence of heat transport. From this work, it is sensed that the flow behavior of the heat rate transmission is higher in the case of suction, and the injection parameter is higher. Ramzan *et al.* [19] analyzed the velocity and thermal slip conditions in a hybrid nanoliquid flow along with Joule heating effect *via* an extended sheet. Raja *et al.* [20] examined the radiative heat and mass flux over the flow of three-dimensional hybrid nanoliquid on the shrinkable surface. In this inquiry, it is noticed that the radiative heat flux parameter enhanced the hybrid nanoliquid temperature. Alsaedi *et al.* [21] dissected the thermophysical properties of the hybrid nanoliquid between the two coaxial cylinders through the occurrence of the magnetic field. Khashi'ie *et al.* [22] made the numerical solution of the flow of hybrid nanofluid with magnetic Reynolds number under the permeable flat plate by using the bvp4c technique. They explained that the rate of heat transport of the working fluid is boosted by the Joule heating effect. Khan *et al.* [23] reviewed the presence of heat source/sink over the mixed convection flow of hybrid nanoliquid induced by the vertical porous cylinder. From their concluding remarks, it is perceived that the curvature parameter of the fluid augmented the drag force.

A new class of fluid is formed when three different kinds of nanoparticles are mixed up in a single base liquid known as the ternary hybrid nanoliquid. The ternary hybrid nanoliquid showed more satisfactory results on the thermal performance of the base liquid as compared to the hybrid nanofluid, nanofluid, and regular fluid. As a result, the ternary hybrid nanofluid is being used by scientists and researchers as a major in their field of study. Khan *et al.* [24] debated the phenomena of ohmic heating and suction over the stagnation point flow of ternary hybrid nanoliquid through the existence of a magnetic effect on the stretching/shirking cylinder. They found that the

Nusselt number of the fluid is heightened by intensifying the number of the nanoparticles in a base liquid. Manjunatha *et al.* [25] explained the behavior of the chemical reaction and thermal conductivity on the MHD flow of ternary hybrid nanoliquid in a stretched sheet. For the numerical solution of their problem, they employed RRKF-45 scheme in their mathematical modeling. Animasaun *et al.* [26] dissected the role of magnetic flux density and heat source/sink over the flow of ternary hybrid nanoliquid under the heated surface. Nazir *et al.* [27] demonstrated the idea of the non-Fourier laws on the flow of pseudo-plastic ternary hybrid nanoliquid in a porous medium passing through the heated surface. Elnaqeeb *et al.* [28] explored the importance of dual stretching and suction on the three-dimensional flow of ternary hybrid nanoliquid through the rectangular closed area with various shapes and densities. Their concluding remarks indicated that the temperature of the ternary hybrid nanoliquid is lower for stretching and suction parameters.

From the past few years, the scientists and researchers pay their attention to the study of the Hall current because of their useful applications in the different fields of manufacturing and industries. Across an electrical conductor, the Hall effect is the generation of a voltage difference that is perpendicular to the current and transverse to the employed magnetic field. Hall current is used in magnetic field equipment, for the measurement of direct current, measurement of phase angles, *etc*. Because of its applications in several fields of engineering and manufacturing, Hall current has become a very interesting aspect for scientists and researchers. Raja *et al.* [29] investigated the boundary layer flow problem in the attendance of thermal radiation and Hall current toward the stretching sheet and they employed the adomian decomposition method numerical procedure for the numerical manipulation of their modeling. Das *et al.* [30] presented the MHD flow of three-dimensional Carreau-nanofluid under the effect of heat generation and Hall current by using the stretchable surface. In this analysis, it is viewed that the heat generation parameter enlarged the nanoliquid temperature. Hussain *et al.* [31] illustrated the effect of Hall current on the MHD flow of mixed convection liquid with chemical reaction embedded in a moving plate through the porous media. Rasheed *et al.* [32] considered the existence of Hall current and heat source/sink over the MHD flow of Casson fluid under the vertical moving surface and observed that the speed of the fluid particles is higher when the Casson parameter is larger. Li *et al.* [33] conducted a study on the peristaltic transport flow of Jeffrey nanoliquid due to the wave frame with viscous dissipation and Hall current. Khan *et al.* [34] discussed the mathematical framework of Hall current and thermal conductivity on the chemically reactive flow of nanoliquid toward the moving thin needle. From their conclusions, it is noticed that the intensification in Lewis number enhanced the fluid concentration.

Scientists and academicians are increasingly interested in studying the processes of heat transfer in various flow situations. Heat can be transferred in three different ways such as conduction, radiation, and convection. Applications of the heat transport are extrusion, blow modeling, batch reactor, continuous processes, catalysis, gas processing, printing, laminating, engineering woods, die temperature control, stream generator, flatwork ironers, roofing material, rolls, synthesis, continuous processes, poultry, hot-mix paying refineries, *etc*. Because of their applicability in various fields of engineering and industries, scientists, researchers, and mathematicians are increasingly interested in studying heat transfer in their various models. Khazayinejad and Nourazar [35] analyzed the flow of hybrid nanoliquid toward the permeable plate with heat transport and discussed the physical features of the graphene oxide (GO) and silver nanoparticles in base fluid water. Arif *et al.* [36] described the flow of ternary hybrid nanoliquid by using three different shaped nanoparticles with heat transport phenomena between the two parallel plates. Rehman *et al.* [37] discovered the magnetohydrodynamic flow of thermally stratified Jeffrey liquid with heat transport and thermal radiation above the cylindrical and plane surface. In this work, they obtained that on a cylindrical surface the rate of heat transmission is larger as compared to the plane surface. Rasheed *et al.* [38] examined the heat transport behavior by using the three-dimensional Brownian motion of the flow of thin film nanoliquid in a stretching surface. From this examination, it is clear that the Sherwood number of the nanofluid is lower with the enhancement of the viscosity parameter. Farooq *et al.* [1] offered the upshot of Cattaneo–Christov heat flux on the nanoliquid flow with the applications of melting heat transport in the attendance of thermal radiation under the stretched sheet. Li *et al.* [2] explicated the role of heat transport and chemical reaction in a time-dependent flow of MHD nanoliquid under the perpendicular plate. This inquiry examined that the rate of heat transportation is more significant in the case of nanoliquid as compared to the regular fluid. Shoaib *et al.* [39] considered the thermal analysis of the heat transport and dipole effect on the two-dimensional flow of ferroliquid due to the exponentially stretchable sheet. Arif *et al.* [40] assessed the engineering applications of the engine oil base fluid by using the Casson liquid

model with ramped wall temperature under the oscillating plate. The exact solution of their mathematical frame work is obtained with the implementation of the Laplace and Fourier transformations. Bejawada *et al.* [41] scrutinized the influence of thermal radiation and Brownian diffusivity in the two-dimensional mixed convection flow of nanofluid with heat transport over the inclined wavy surface. Alkathiri *et al.* [42] presented the impacts of the entropy generation and viscous dissipation on the Casson nanoliquid flow with heat transport, and in this study, they used engine oil as a base liquid and Cu and ferro (Fe_3O_4) are the nanoparticles. Eid and Mabood [43] discussed the behavior of the heat transport and Darcy–Forchheimer over the MHD micropolar nanoliquid flow toward the stretchable surface. They identified that the microrotation profile of the nanoliquid is greater for the magnetic field parameter. Parvin *et al.* [44] dissected the problem of Maxwell nanofluid flow under the inclined surface with the heat and mass transportation phenomena. In this inspection, it is clear that the speed of the fluid particles is lower due to the augmentation of the nanoparticle volume fraction. Further research on the heat transport mechanism can be found in refs [45–50].

In the view of the abovementioned literature, the present problem describes the three-dimensional MHD flow of ternary hybrid nanoliquid in the attendance of Hall current and Darcy–Forchheimer toward the rotating porous surface. In heat equation, the phenomena of heat transport are discussed. For the manipulation of mass transmission, the chemical reaction and activation energy are considered in the current analysis. The whole problem is scrutinized under the convective conditions. Homotopic scheme is exploited for the analytical simulation of the present problem. The nature of discrete flow parameters over the velocities, temperature, and concentration of the ternary hybrid nanoliquid are discussed in a graphical form with a detailed physical description. The skin friction coefficients, Nusselt number, and Sherwood number are investigated for distinct flow parameters. The practical applications of the present work at an industrial and engineering level are the condensation process of a metallic plate in a glass, glass fiber production, polymer industries, in a bath, aerodynamic extrusion of the plastics sheets, and many others.

2 Problem formulation

The thermal performance of the three-dimensional MHD flow of ternary hybrid nanoliquid in the presence of Darcy–Forchheimer medium toward a rotating surface is considered here. The steady and incompressible flow is assumed to be study in this analysis. For the analysis of the flow behavior of tri-hybrid nanoparticles, the law of ion-slip force and Hall current are also taken into consideration. The significance of the chemical reaction and activation energy are elaborated in the current analysis. On the basis of the tri-hybrid nanoparticles, a new theoretical framework is implemented. In this investigation, the GO, Ag, and Cu nanoparticles are considered, whereas the kerosene oil is considered as a base fluid. $\bar{T}$ is the nanoliquid temperature, $\bar{T}_w$ is the surface temperature, and $\bar{T}_\infty$ is the ambient temperature. In case of mass equation, $\bar{C}$ is the concentration, $\bar{C}_w$ is the surface concentration, and $\bar{C}_\infty$ is the ambient concentration. The present problem is modeled by keeping in mind the abovementioned assumption of the flow behavior; the leading equations are defined as (Figure 1):

$$\frac{\partial \bar{u}}{\partial x} + \frac{\partial \bar{v}}{\partial y} + \frac{\partial \bar{w}}{\partial z} = 0, \tag{1}$$

$$\begin{aligned} &\bar{u}\frac{\partial \bar{u}}{\partial x} + \bar{v}\frac{\partial \bar{u}}{\partial y} + \bar{w}\frac{\partial \bar{u}}{\partial z} - 2\omega\bar{v} \\ &= \nu_{Thnf}\frac{\partial^2 \bar{u}}{\partial z^2} - \frac{\nu_{Thnf}}{k^*}F_s\bar{u} - \frac{F_s}{\sqrt{k^*}}\bar{u}^2 \\ &\quad + \frac{B_0^2\sigma_{Thnf}}{\rho_{Thnf}[\gamma_e^2 + (1+\gamma_e\gamma_i)^2]}[\gamma_e\bar{v} - (1+\gamma_e\gamma_i)\bar{u}], \end{aligned} \tag{2}$$

$$\begin{aligned} &\bar{u}\frac{\partial v}{\partial x} + \bar{v}\frac{\partial \bar{v}}{\partial y} + w\frac{\partial \bar{v}}{\partial z} + 2\omega\bar{u} \\ &= \nu_{Thnf}\frac{\partial^2 \bar{v}}{\partial z^2} - \frac{\nu_{Thnf}}{k^*}F_s\bar{v} - \frac{F_s}{\sqrt{k^*}}\bar{v}^2 \\ &\quad + \frac{B_0^2\sigma_{Thnf}}{\rho_{Thnf}[\gamma_e^2 + (1+\gamma_e\gamma_i)^2]}[\gamma_e\bar{u} + (1+\gamma_e\gamma_i)\bar{v}], \end{aligned} \tag{3}$$

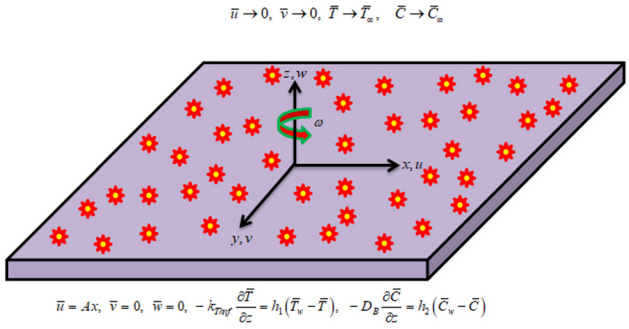

Figure 1: Flow geometry.

$$\bar{u}\frac{\partial \bar{T}}{\partial x} + \bar{v}\frac{\partial \bar{T}}{\partial y} + \bar{w}\frac{\partial \bar{T}}{\partial z} = \frac{k_{Thnf}}{(\rho C_p)_{Thnf}}\frac{\partial^2 \bar{T}}{\partial z^2} + \frac{B_0^2 \sigma_{Thnf}}{(\rho C_p)_{Thnf}[\gamma_e^2 + (1+\gamma_e\gamma_i)^2]}[\bar{u}^2 + \bar{v}^2], \tag{4}$$

$$\bar{u}\frac{\partial \bar{C}}{\partial x} + \bar{v}\frac{\partial \bar{C}}{\partial y} + \bar{w}\frac{\partial \bar{C}}{\partial z} + k_c^2(\bar{C} - \bar{C}_\infty)\left(\frac{\bar{T}}{\bar{T}_\infty}\right)^n \exp\left(\frac{-E_a}{k_B \bar{T}}\right) = D_B\frac{\partial^2 \bar{C}}{\partial z^2}. \tag{5}$$

The boundary conditions are as follows:

$$\left.\begin{aligned} &\bar{u} = Ax,\ \bar{v} = 0,\ \bar{w} = 0,\ -k_{Thnf}\frac{\partial \bar{T}}{\partial z} = h_1(\bar{T}_w - \bar{T}),\\ &-D_B\frac{\partial \bar{C}}{\partial z} = h_2(\bar{C}_w - \bar{C})\ at\ z = 0\\ &\bar{u} \to 0,\ \bar{v} \to 0,\ \bar{T} \to \bar{T}_\infty, \bar{C} \to \bar{C}_\infty\ \text{as}\ z \to \infty \end{aligned}\right\}, \tag{6}$$

where the velocity components in x-, y-, and z-directions are $\bar{u}$, $\bar{v}$, and $\bar{w}$, respectively; the kinematics viscosity of the ternary hybrid nanoliquid is ν_{Thnf}; the permeability of the porous media is $k^\star$; F_s is the coefficient of inertia related to the porous medium; density of the ternary hybrid nanoliquid is ρ_{Thnf}; B_0 is the magnetic field strength; the electrical conductivity of the ternary hybrid nanoliquid is σ_{Thnf}; γ_e is the Hall current; the ion-slip number is γ_i; the ternary hybrid nanoliquid thermal conductivity is k_{Thnf}; the specific heat is C_p; the chemical reaction rate is k_c; the power index is n; and E_a is the activation energy.

The following are the similarity transformations for the current problem:

$$\bar{u} = AxF',\ \bar{v} = AxG,\ \bar{w} = -F(A\nu_f)^{\frac{1}{2}},\ \xi = \left(\frac{A}{\nu_f}\right)^{\frac{1}{2}}z,\quad \theta = \frac{\bar{T} - \bar{T}_\infty}{\bar{T}_w - \bar{T}_\infty},\ \phi = \frac{\bar{C} - \bar{C}_\infty}{\bar{C}_w - \bar{C}_\infty}. \tag{7}$$

The thermophysical characteristics of the base liquid and nanoparticles are listed in Table 1.

Table 1: Thermophysical characteristics of the nanoparticles and base liquid

Physical property	GO	Ag	Cu	Kerosene oil
ρ (kg/m^3)	1,800	10,500	632	783
C_p (J/kg K)	717	235	531.8	2,090
σ (Ωm)	6.30 $\times 10^7$	63×10^{-6}	5.96 $\times 10^7$	21×10^{-6}
k (W/mK)	5,000	429	765	0.145

The thermophysical characteristics of the nanofluid, hybrid nanoliquid, and ternary hybrid nanoliquid are, respectively, discussed as:

$$\left.\begin{aligned} &\frac{\mu_{nf}}{\mu_f} = \frac{1}{(1-\phi_1)^{2.5}},\ \frac{\rho_{nf}}{\rho_f} = (1-\phi_1) + \frac{\rho_1\phi_1}{\rho_f},\\ &\frac{(\rho C_p)_{nf}}{(\rho C_p)_f} = (1-\phi_1) + \frac{(\rho C_p)_1\phi_1}{(\rho C_p)_f},\\ &\frac{\sigma_{nf}}{\sigma_f} = 1 + \frac{3\left[\left(\frac{\sigma_1}{\sigma_f} - 1\right)\phi_1\right]}{\left(\frac{\sigma_1}{\sigma_f} + 2\right) - \left(\frac{\sigma_1}{\sigma_f} - 1\right)\phi_1},\ \frac{k_{nf}}{k_f} = 1 + \frac{3\left[\left(\frac{k_1}{k_f} - 1\right)\phi_1\right]}{\left(\frac{k_1}{k_f} + 2\right) - \left(\frac{k_1}{k_f} - 1\right)\phi_1}. \end{aligned}\right\} \tag{8}$$

$$\left.\begin{aligned} &\frac{\mu_{hnf}}{\mu_f} = \frac{1}{(1-\phi_1-\phi_2)^{2.5}},\ \frac{\rho_{hnf}}{\rho_f} = (1-\phi_2)\left[(1-\phi_2) + \frac{\rho_1\phi_1}{\rho_f}\right] + \frac{\rho_2\phi_2}{\rho_f}\\ &\frac{(\rho C_p)_{hnf}}{(\rho C_p)_f} = (1-\phi_2)\left[(1-\phi_1) + \frac{(\rho C_p)_1\phi_1}{(\rho C_p)_f}\right] + \frac{(\rho C_p)_2\phi_2}{(\rho C_p)_f},\\ &\frac{\sigma_{hnf}}{\sigma_f} = 1 + \frac{3\left(\frac{\sigma_1\phi_1 + \sigma_2\phi_2}{\sigma_f}\right) - 3(\phi_1+\phi_2)}{2 + \left\{\frac{\sigma_1\phi_1 + \sigma_2\phi_2}{(\phi_1+\phi_2)\sigma_f}\right\} - \left\{\frac{\sigma_1\phi_1 + \sigma_2\phi_2}{\sigma_f} - (\phi_1+\phi_2)\right\}},\\ &\frac{k_{hnf}}{k_f} = \frac{\frac{k_1\phi_1 + k_2\phi_2}{\phi_1+\phi_2} + 2k_f + 2(k_1\phi_1 + k_2\phi_2) - 2(\phi_1+\phi_2)k_f}{\frac{k_1\phi_1 + k_2\phi_2}{\phi_1+\phi_2} + 2k_f - 2(k_1\phi_1 + k_2\phi_2) + (\phi_1+\phi_2)k_f}, \end{aligned}\right\} \tag{9}$$

$$\left.\begin{aligned} &\mu_{Thnf} = \frac{\mu_f}{(1-\phi_1)^{2.5}(1-\phi_2)^{2.5}(1-\phi_3)^{2.5}},\\ &\rho_{Thnf} = (1-\phi_1)\{(1-\phi_2)[(1-\phi_3)\rho_f + \rho_3\phi_3] + \rho_2\phi_2\} + \rho_1\phi_1,\\ &\frac{(\rho C_p)_{Thnf}}{(\rho C_p)_f} = \frac{(\rho C_p)_1\phi_1}{(\rho C_p)_f} + (1-\phi_1)\left[(1-\phi_2)\left\{(1-\phi_3) + \frac{(\rho C_p)_3\phi_3}{(\rho C_p)_f}\right\} + \frac{(\rho C_p)_2\phi_2}{(\rho C_p)_f}\right],\\ &\frac{\sigma_{Thnf}}{\sigma_{hnf}} = \frac{\sigma_1(1+2\phi_1) + \sigma_{hnf}(1-2\phi_1)}{\sigma_1(1-\phi_1) + \sigma_{hnf}(1+\phi_1)},\ \frac{\sigma_{hnf}}{\sigma_{nf}} = \frac{\sigma_2(1+2\phi_2) + \sigma_{nf}(1-2\phi_2)}{\sigma_2(1-\phi_2) + \sigma_{nf}(1+\phi_2)},\\ &\frac{\sigma_{nf}}{\sigma_f} = \frac{\sigma_3(1+2\phi_3) + \sigma_f(1-2\phi_3)}{\sigma_3(1-\phi_3) + \sigma_f(1+\phi_3)},\ \frac{k_{Thnf}}{k_{hnf}} = \frac{k_1 + 2k_{hnf} - 2\phi_1(k_{hnf} - k_1)}{k_1 + 2k_{hnf} + \phi_1(k_{hnf} - k_1)},\\ &\frac{k_{hnf}}{k_{nf}} = \frac{k_2 + 2k_{nf} - 2\phi_2(k_{nf} - k_2)}{k_2 + 2k_{nf} + \phi_2(k_{nf} - k_2)},\ \frac{k_{nf}}{k_f} = \frac{k_3 + 2k_f - 2\phi_3(k_f - k_3)}{k_3 + 2k_f + \phi_3(k_f - k_3)}, \end{aligned}\right\} \tag{10}$$

In Eqs. (8–10), ϕ denotes the volume fraction of the nanoparticles and the subscripts 1, 2, 3 denote the first, second, and third nanoparticle, respectively.

Using Eq. (7), Eqs. (2–5) are transformed as:

$$\frac{\mu_{Thnf}/\mu_f}{\rho_{Thnf}/\rho_f}F''' + (FF'' - (F')^2) + 2G\ \Omega - \frac{\mu_{Thnf}/\mu_f}{\rho_{Thnf}/\rho_f}\varepsilon F' - \mathrm{Fr}F'^2 + \frac{\sigma_{Thnf}/\sigma_f}{\rho_{Thnf}/\rho_f}\frac{M}{\{\gamma_e^2 + (1+\gamma_e\gamma_i)^2\}}\{\gamma_e G - (1+\gamma_e\gamma_i)F'\} = 0, \tag{11}$$

$$\frac{\mu_{Thnf}/\mu_f}{\rho_{Thnf}/\rho_f}G'' + (FG' - F'G) - 2F'\ \Omega - \frac{\mu_{Thnf}/\mu_f}{\rho_{Thnf}/\rho_f}\varepsilon G - \mathrm{Fr}G^2 - \frac{\sigma_{Thnf}/\sigma_f}{\rho_{Thnf}/\rho_f}\frac{M}{(\gamma_e^2 + (1+\gamma_e\gamma_i)^2)}(\gamma_e F' + (1+\gamma_e\gamma_i)G) = 0, \tag{12}$$

$$\frac{k_{Thnf}/k_f}{(\rho C_p)_{Thnf}/(\rho C_p)_f}\theta'' + \mathrm{Pr}F\theta' + \left(\frac{\sigma_{Thnf}/\sigma_f}{(\rho C_p)_{Thnf}/(\rho C_p)_f}\right)\frac{M\mathrm{PrEc}}{(\gamma_e^2 + (1+\gamma_e\gamma_i)^2)}(F'^2 + G^2) = 0, \tag{13}$$

$$\phi'' + \mathrm{Sc}f\phi' + \mathrm{krSc}\phi(\delta\theta + 1)^n \exp\left[\frac{-E}{(\delta\theta + 1)}\right] = 0, \tag{14}$$

The transformed boundary conditions are as follows:

$$\left.\begin{aligned} &F(0) = 0,\ F'(0) = 1,\ G(0) = 0,\\ &\frac{k_{Thnf}}{k_f}\theta'(0) = -Bi_T(1 - \theta(0)),\\ &\phi'(0) = -Bi_C(1 - \phi(0)),\\ &F'(\infty) = 0,\ G(\infty) = 0,\ \theta(\infty) = 0,\ \phi(\infty) = 0. \end{aligned}\right\} \tag{15}$$

The different flow parameters in dimensionless form are discussed here. The rotation parameter is represented by $\Omega\left(=\frac{\omega}{\nu_f}\right)$, the Prandtl number is denoted by $\mathrm{Pr}\left(=\frac{(C_p)_f\mu_f}{k_f}\right)$, Darcy–Forchheimer parameter is indicated by $\mathrm{Fr}\left(=\frac{F_s x}{\sqrt{k^*}}\right)$, porosity parameter is specified by $\varepsilon\left(=\frac{\nu_f F_s}{k^* A}\right)$, the Eckert number is $\mathrm{Ec}\left(=\frac{u_w^2}{(C_p)_f(\bar{T}_w - \bar{T}_\infty)}\right)$, the magnetic field parameter is $M\left(=\frac{B_0^2\sigma_f}{A\rho_f}\right)$, the chemical reaction parameter is denoted by $\mathrm{kr}\left(=\frac{k_c^2}{A}\right)$, the Schmidt number is designated by $\mathrm{Sc}\left(=\frac{\nu_f}{D_B}\right)$, the activation energy is $E\left(=\frac{E_a}{\bar{T}_\infty k_B}\right)$, the temperature difference is represented by $\delta\left(=\frac{(\bar{T}_w - \bar{T}_\infty)}{\bar{T}_\infty}\right)$, the thermal Biot number is signified by $\mathrm{Bi_T}\left(=\frac{h_1}{k_f}\sqrt{\frac{\nu_f}{A}}\right)$, and the solutal Biot number is $\mathrm{Bi_C}\left(=\frac{h_2}{D_B}\sqrt{\frac{\nu_f}{A}}\right)$.

The dimensionless form of the skin friction coefficients in x- and y-directions, Nusselt number, and Sherwood number are defined as:

$$C_x = \mathrm{Re}_x^{\frac{1}{2}}Cf_x = \frac{\mu_{Thnf}}{\mu_f}F''(0), \tag{16}$$

$$C_y = \mathrm{Re}_y^{\frac{1}{2}}Cf_y = \frac{\mu_{Thnf}}{\mu_f}G'(0), \tag{17}$$

$$\mathrm{Nu} = \mathrm{Re}_x^{-\frac{1}{2}}\mathrm{Nu}_x = -\frac{k_{Thnf}}{k_f}\theta'(0), \tag{18}$$

$$\mathrm{Sh} = \mathrm{Re}_x^{-\frac{1}{2}}\mathrm{Sh}_x = -\phi'(0). \tag{19}$$

3 Solution of the problem

The homotopic analysis scheme is utilized for the analytical simulation of the higher order nonlinear ordinary differential equations (ODEs). The homotopy analysis method (HAM) has a lot of advantages over the other methods. Hence, the HAM is preferred for the analytical solution of the current problem. The following are some of the advantages of homotopy analysis scheme:

- It is a method of series expansion that is independent of small or large physical parameters.
- The HAM is not only used for the simulation of weakly nonlinear problems, but it is also used for strongly nonlinear problems.
- This method can be exploited to any system of nonlinear differential equations without the need for linearization and discretization.
- This approach does not require any base functions or linear operators.

The initial guesses are defined as:

$$\begin{aligned} F_0(\xi) &= 1 - \mathrm{e}^{-\xi},\ G_0(\xi) = 0,\\ \theta_0(\xi) &= \frac{k_{Thnf}}{k_f}\left(\frac{\mathrm{Bi_T}}{1 + \mathrm{Bi_T}}\right)\mathrm{e}^{-\xi},\\ \phi_0(\xi) &= \left(\frac{\mathrm{Bi_C}}{1 + \mathrm{Bi_C}}\right)\mathrm{e}^{-\xi}. \end{aligned} \tag{20}$$

Linear operators are taken as:

$$\begin{aligned} \mathbf{L}_F(\xi) &= F''' - F',\ \mathbf{L}_G(\xi) = G'' - G,\\ \mathbf{L}_\theta(\xi) &= \theta'' - \theta,\ \mathbf{L}_\phi(\xi) = \phi'' - \phi, \end{aligned} \tag{21}$$

with properties:

$$\left.\begin{aligned} &\mathbf{L}_F(C_1 + C_2\exp(\xi) + C_3\exp(-\xi)) = 0,\\ &\mathbf{L}_G(C_4\exp(\xi) + C_5\exp(-\xi)) = 0,\\ &\mathbf{L}_\theta(C_6\exp(\xi) + C_7\exp(-\xi)) = 0,\\ &\mathbf{L}_\phi(C_8\exp(\xi) + C_9\exp(-\xi)) = 0, \end{aligned}\right\} \tag{22}$$

where $C_i (i = 1 - 9)$ are the constants.

4 Convergence of HAM

The series solution of the current model is attained by applying the HAM scheme. The convergence region of the model is adjustable and controllable with the assistance of auxiliary parameter $\hbar$. The $\hbar$-curves of the $F''(0)$, $G'(0)$, $\theta'(0)$, and $\phi'(0)$ are schemed in Figure 2.

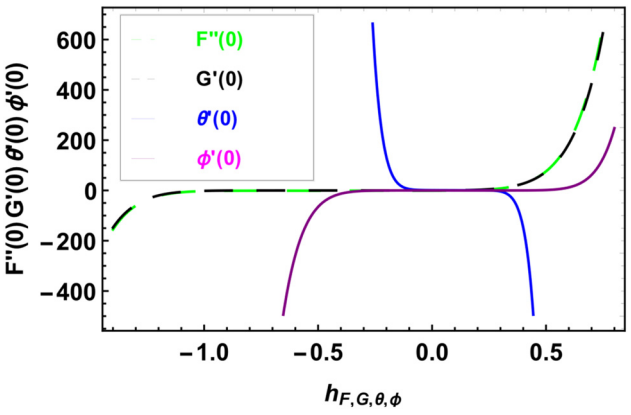

Figure 2: $\hbar$-curves for $F''(0)$, $G'(0)$, $\theta'(0)$, and $\phi'(0)$.

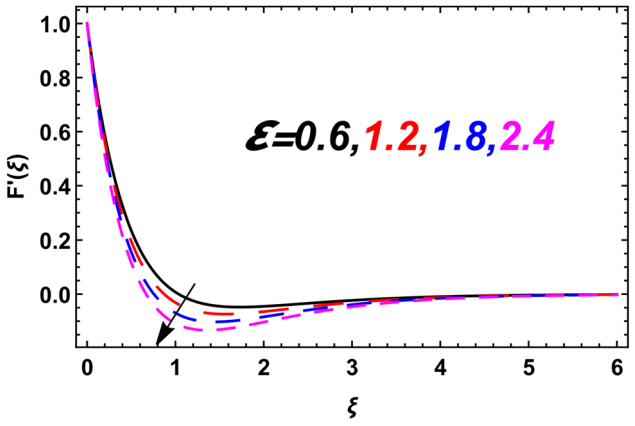

Figure 3: Variation in the ternary hybrid nanofluid velocity due to ε.

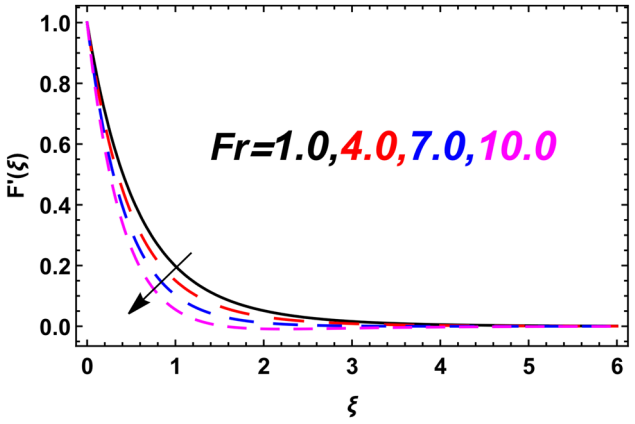

Figure 4: Variation in the ternary hybrid nanofluid velocity due to Fr.

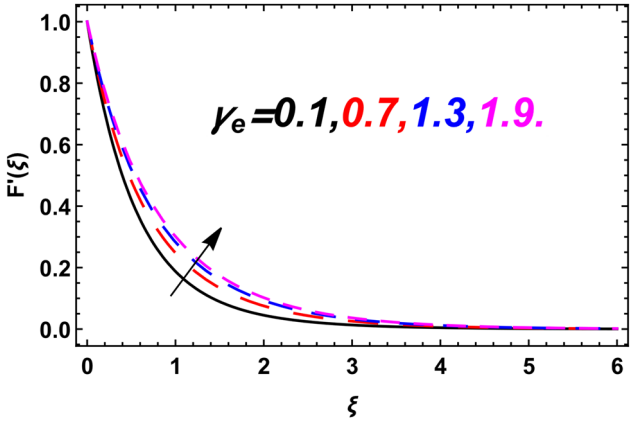

Figure 5: Variation in the ternary hybrid nanofluid velocity due to γ_e.

The convergence region for $F''(0)$, $G'(0)$, $\theta'(0)$, and $\phi'(0)$ are $-1.2 \le \hbar_F \le 0.5$, $-1.2 \le \hbar_G \le 0.5$, $-0.1 \le \hbar_\theta \le 0.4$, and $-0.5 \le \hbar_\phi \le 0.7$, respectively.

5 Results and discussion

In this segment, the impacts of physical parameters on the ternary hybrid nanoliquid flow profiles are presented. For the analytical simulation of the current analysis, the homotopic analysis scheme is considered. The influences of the discrete flow parameters over the velocities in x- and y-directions, temperature, and concentration of the ternary hybrid nanoliquid are computed and discussed in a schematic form with detailed physical explanation.

5.1 Velocity profiles in x-direction

Figures 3–7 demonstrate the influences of different flow parameters such as porosity parameter ε, Darcy-Forchheimer parameter Fr, Hall current parameter γ_e, ion-slip number γ_i, and magnetic parameter M on the ternary hybrid nanoliquid velocity in x-direction. The fluctuation in the velocity of the ternary hybrid nanoliquid for higher estimation of porosity parameter ε is offered in Figure 3. From this inspection, it is detected that intensifying the values of ε reduced the ternary hybrid nanofluid velocity. The behavior of Darcy–Forchheimer parameter Fr over the velocity of the ternary hybrid nanoliquid is explained in Figure 4. In Figure 4, it is observed that the ternary hybrid nanoliquid velocity is lower for Darcy–Forchheimer parameter Fr. The thickness of the motion of the liquid particles is enhanced due to the intensification of Darcy–Forchheimer parameter. When the idea of Forchheimer is recognized, then the force of retardation is predicted. A nonlinear relationship exists between Darcy–Forchheimer flow and fluid flow. By using the

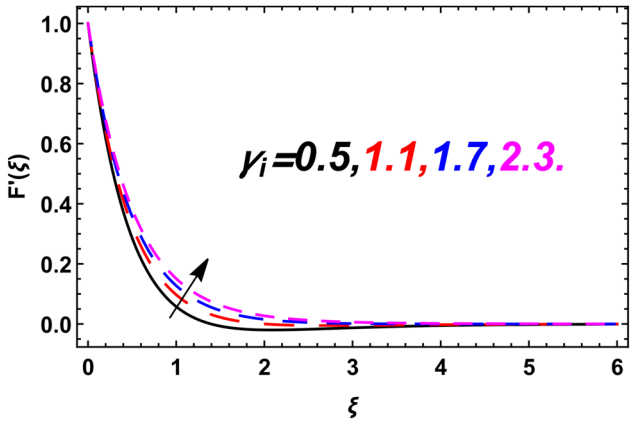

Figure 6: Variation in the ternary hybrid nanofluid velocity due to γ_i.

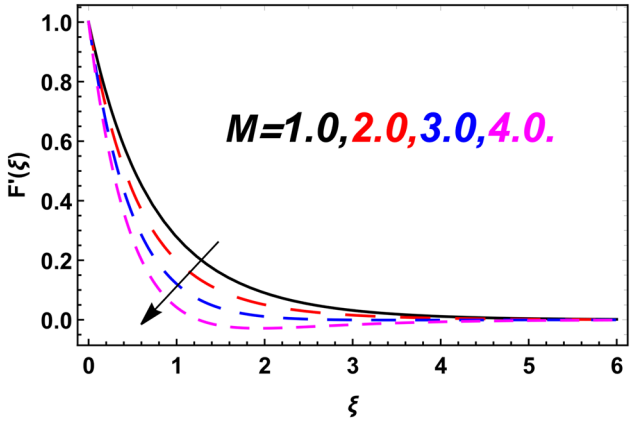

Figure 7: Variation in the ternary hybrid nanofluid velocity due to M.

Darcy–Forchheimer theory, the Darcy–Forchheimer parameter is formulated. Furthermore, the porosity of the sheet and Darcy-Forchheimer are associated with each other. Thus, the liquid motion is lower due to the porosity of the sheet and hence the velocity of the ternary hybrid nanoliquid is lower. Figure 5 analyzes the role of Hall current parameter γ_e over the velocity of the ternary hybrid nanoliquid. In this figure, the enhancement in the velocity of the ternary hybrid nanoliquid is noticed due to the varying values of the Hall current parameter γ_e. Basically, the generalized Ohm's theory is responsible for the formation of Hall number. Also, the momentum and energy equations contain the Hall current behavior. By the improvement of the Hall current, a Lorentz force is created in between the fluid particles. The relation between the flow distribution and Hall current is directly to each other. Thus, the speed of the fluid particles is amplified due to the increase in the Hall parameter. The influence of the ion-slip number γ_i on the velocity of the ternary hybrid nanofluid is determined in Figure 6. The increment in the ternary hybrid nanoliquid velocity is noted for intensifying estimation of the ion-slip number γ_i. The effect of the magnetic parameter M on the velocity of the ternary hybrid nanoliquid is discussed in Figure 7. From this enquiry, it is distinguished that larger estimation of magnetic parameter M led to diminish the velocity of the ternary hybrid nanoliquid. Because when magnetic parameter M is greater, the Lorentz force is produced between the particles of the liquid which slows down the motion of the liquid particles and thus, the velocity of the ternary hybrid nanofluid is diminished. Also, it is examined that due to the surge of magnetic parameter, a large amount of frictional force between the fluid particles is created. Physically the rate of heat transport is enhanced due to the production of Lorentz force that decreased the velocity of the ternary hybrid nanoliquid.

5.2 Velocity profile in y-direction

Figures 8–11 explain the variations in ternary hybrid nanofluid velocity *versus* distinct flow parameters such as Hall current γ_e, ion-slip number γ_i, magnetic parameter M, and rotation parameter Ω. Figure 8 portrays the effect of Hall current γ_e on the velocity of the ternary hybrid nanoliquid. The augmentation in the ternary hybrid nanoliquid velocity is inspected with the escalating values of Hall current γ_e. Basically, the generalized Ohm's theory is responsible for the formation of the Hall number. Also, the momentum and energy equations contain the Hall current behavior. By the improvement of the Hall current, a Lorentz force is created in between the fluid particles. The relation between the flow distribution and Hall current is directly to each other. Thus, the speed of the fluid particles is amplified

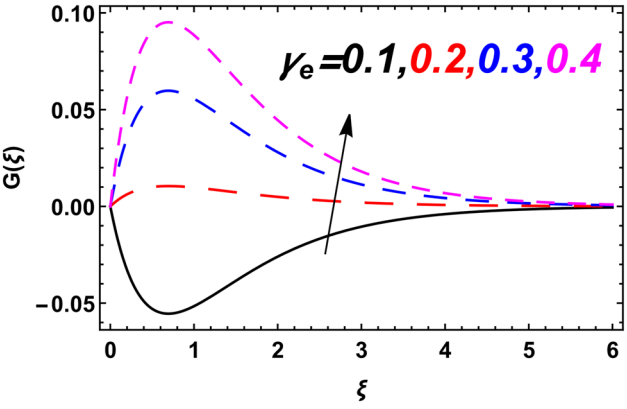

Figure 8: Variation in ternary hybrid nanofluid velocity due to γ_e.

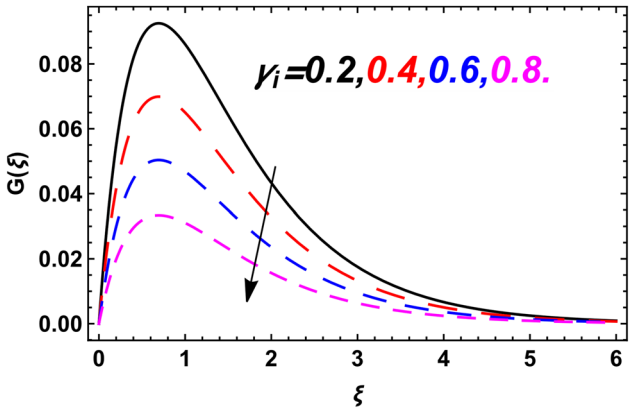

Figure 9: Variation in the ternary hybrid nanofluid velocity due to γ_i.

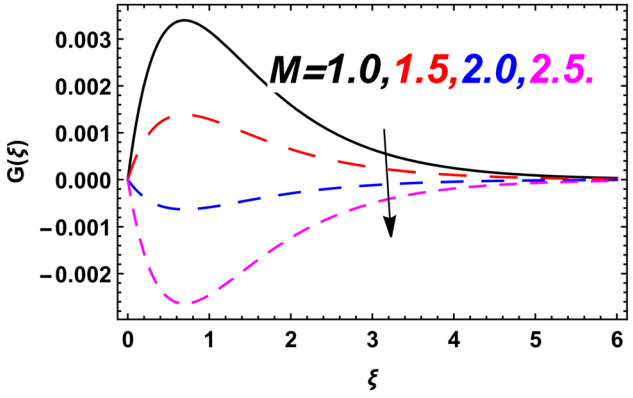

Figure 10: Variation in the ternary hybrid nanofluid velocity due to M.

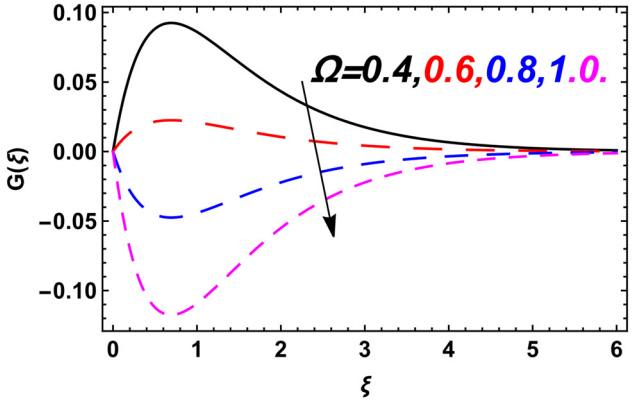

Figure 11: Variation in the ternary hybrid nanofluid velocity due to Ω.

due to the increase in the Hall parameter. The impact of ion-slip number γ_i over the velocity of the ternary hybrid nanoliquid is inspected in Figure 9. It is clear that the rising values of the ion-slip number γ_i weaken the ternary hybrid nanoliquid velocity. The result of the magnetic parameter M on the ternary hybrid nanoliquid velocity is described in Figure 10. In Figure 10, the decrement behavior in the ternary hybrid nanofluid velocity against expanding estimation of the magnetic parameter M is observed. Figure 11 examines the behavior of the ternary hybrid nanoliquid velocity for greater values of the rotation parameter Ω. From this inspection, it is detected that the velocity of the ternary hybrid nanoliquid in y-direction is reduced due to the increase in rotation parameter Ω.

5.3 Temperature profile

The graphical analysis of the temperature of the ternary hybrid nanofluid against thermal Biot number Bi_T, Eckert number Ec, Hall current parameter γ_e, ion-slip parameter γ_i, and magnetic parameter M is deliberated in Figures 12–16. Figure 12 discourses the effect of the thermal Biot number Bi_T on the temperature of the ternary hybrid nanoliquid. In Figure 12, it is scrutinized that the intensifying estimation of thermal Biot number Bi_T enhances the temperature of the ternary hybrid nanoliquid. The nature of the ternary hybrid nanoliquid temperature due to the boosting estimation of Eckert number Ec is illustrated in Figure 13. From Figure 13, it is noted that the expanding estimation of Ec upsurges the temperature of the ternary hybrid nanofluid. The relationship between the heat enthalpy variation and kinetic energy of the fluid is termed as the Eckert number. With the enhancement of the Eckert number, the conversion of the mechanical energy into the thermal energy becomes faster and

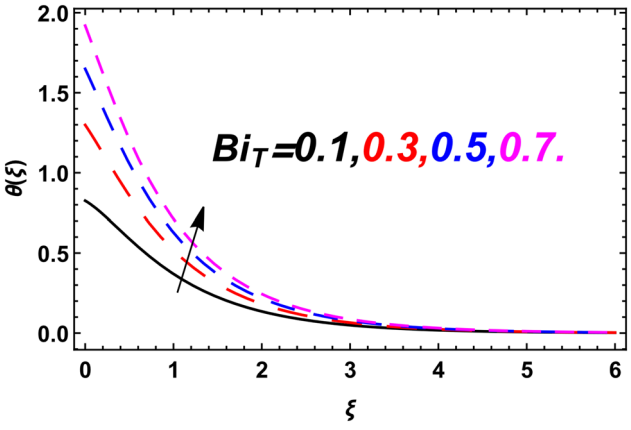

Figure 12: Variation in the ternary hybrid nanofluid temperature due to Bi_T.

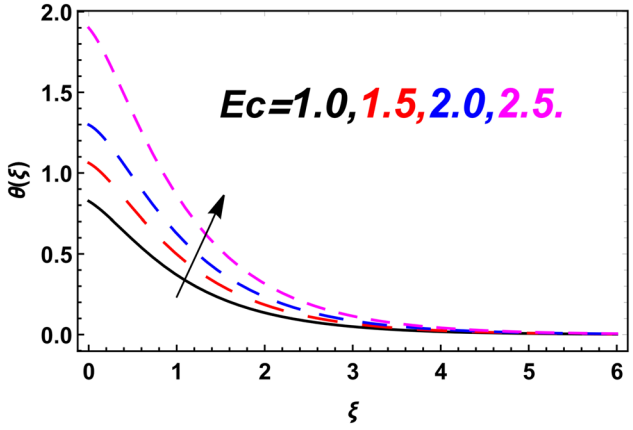

Figure 13: Variation in the ternary hybrid nanofluid temperature due to Ec.

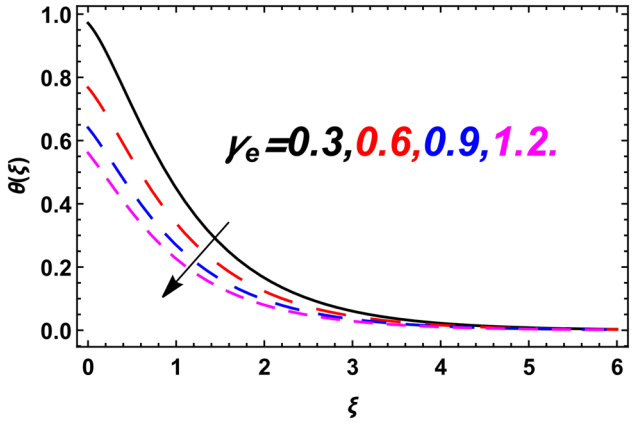

Figure 14: Variation in the ternary hybrid nanofluid temperature due to γ_e.

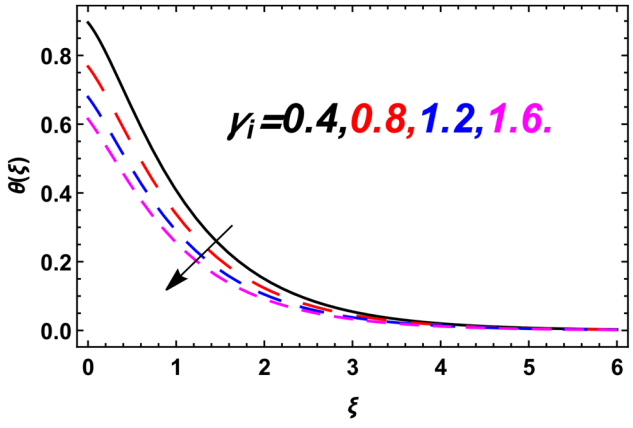

Figure 15: Variation in the ternary hybrid nanofluid temperature due to γ_i.

faster, which causes to enhance the temperature of the ternary hybrid nanofluid. It is detected that the temperature is defined as the average kinetic energy and this

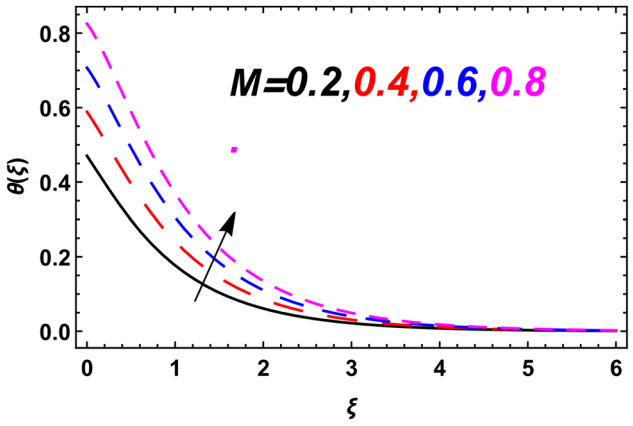

Figure 16: Variation in the ternary hybrid nanofluid temperature due to *M*.

kinetic energy can be augment by the rising Eckert number. Therefore, the ternary hybrid nanoliquid temperature becomes higher due to the increasing Eckert number. The attribute of the Hall current parameter γ_e on the ternary hybrid nanofluid temperature is plotted in Figure 14. For expanding values of Hall current parameter γ_e, the temperature of the ternary hybrid nanoliquid is lessened. Figure 15 is drawn to check the impact of ion-slip parameter $\gamma_i$on the ternary hybrid nanofluid temperature. The decreasing trend in the temperature of the ternary hybrid nanoliquid is detected due to the enhancing values of the ion-slip number γ_i. Due to the existence of the Joule heating effect in energy equation, the Hall current and ion-slip number are modeled. It is noted that due to the enhancing of Hall current and ion-slip number, the thermal profile of the ternary hybrid nanofluid is reduced. Mathematically, in the energy equation, the Hall current and ion-slip number are formulated in the form of Joule heating term and appeared in the denominator. Hence, the relation between the ion-slip number and Hall current heat energy is inverse to each other. Therefore, the Hall current and ion-slip number diminished the temperature of the ternary hybrid nanoliquid. Figure 16 presents the influence of the magnetic parameter *M* on the ternary hybrid nanoliquid temperature. For the rising estimation of the magnetic parameter *M*, the temperature of the ternary hybrid nanoliquid is improved. It is due to the fact that with the increasing magnetic parameter, the thermal boundary layer of the ternary hybrid nanoliquid becomes thinner. Also, the relation between the magnetic field and density of the ternary hybrid nanofluid is inversely proportional. It is clear that the motion of the liquid particles is slow down due to the rising of the magnetic field and then the kinetic energy of

the liquid is converted into the heat energy, and thus, the temperature of the ternary hybrid nanoliquid is enhanced.

5.4 Concentration profile

The outcomes of the ternary hybrid nanofluid concentration for varying values of the temperature difference parameter δ, activation energy E, chemical reaction kr, and Schmidt number Sc are elaborated in Figures 17–20. The impact of the temperature difference parameter δ on the concentration profile of the ternary hybrid nanoliquid is examined in Figure 17. From this analysis, it is perceived that the ternary hybrid nanoliquid concentration is higher for increasing estimation of temperature difference parameter δ. Figure 18 shows the physical significance of the ternary hybrid nanofluid concentration against higher values of activation energy E. The increase in activation energy E enlarges the concentration of the ternary hybrid nanoliquid. In Figure 19, the behavior of the chemical reaction parameter kr over the concentration of the ternary hybrid nanofluid is presented. The transport phenomena of the fluid particles are higher due to the rising of the molecular motion; therefore, the concentration of the fluid is lower for chemical reaction parameter. The upshot of the Schmidt number Sc over the concentration of the ternary hybrid nanoliquid is computed in Figure 20. From this analysis, it is noticed that the ternary hybrid nanofluid concentration becomes lower for larger estimation of the Schmidt number Sc. Actually, the

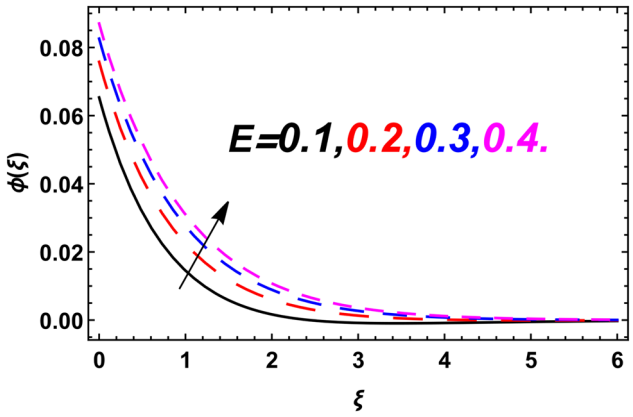

Figure 18: Variation in the ternary hybrid nanofluid concentration due to E.

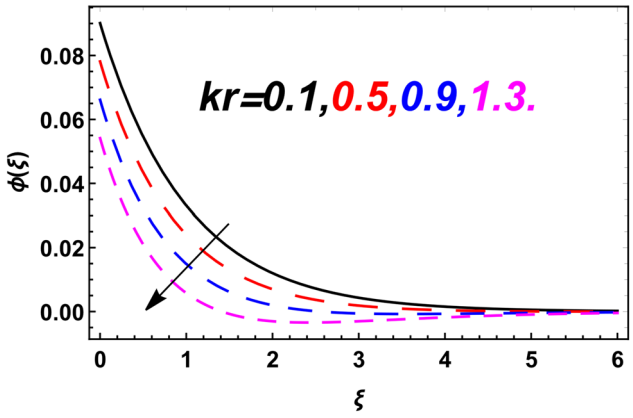

Figure 19: Variation in the ternary hybrid nanofluid concentration due to kr.

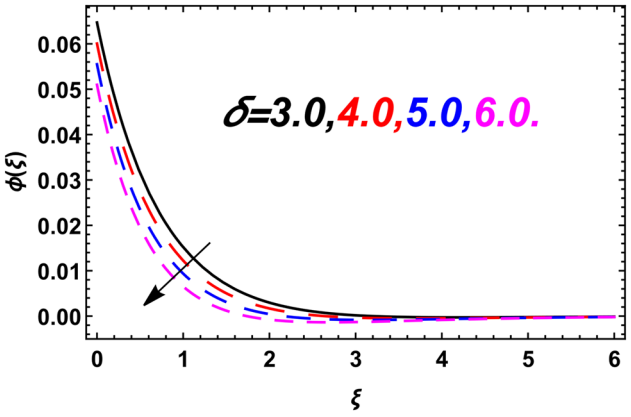

Figure 17: Variation in the ternary hybrid nanofluid concentration due to δ.

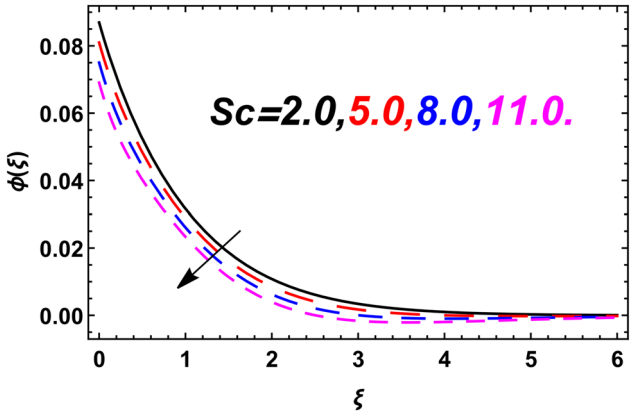

Figure 20: Variation in the ternary hybrid nanofluid concentration due to Sc.

Schmidt number is the ratio between the mass diffusion and viscous forces. The viscous forces of the fluid are increased due to the increase in the Schmidt number but the mass diffusion is decreased. Thus, the concentration of the fluid decreases with the decrease in the mass diffusion.

6 Skin friction coefficient, Nusselt number, and Sherwood number

The graphical analysis of the skin friction coefficient C_x, Nusselt number Nu_x, and Sherwood number Sh_x *via* different flow parameters is discussed in Figures 21–27. Figure 21 determines the impact of the nanoparticle volume fraction ϕ_1 over the skin friction coefficient C_x of the nanoliquid *via* Darcy–Forchheimer parameter Fr. It is distinguished that the GO nanofluid skin friction coefficient C_x is lower *via* Darcy–Forchheimer parameter Fr for intensifying estimation of the nanoparticle volume fraction ϕ_1. In Figure 22, similar effect is noted on the skin friction coefficient C_y of the GO nanofluid for intensifying values of nanoparticle volume fraction ϕ_1. Figures 23 and 24 analyze the role of the nanoparticle volume fraction ϕ_2 in the skin friction coefficients C_x and C_y of the Ag nanofluid. In these graphs, both the skin friction coefficients C_x and C_y of the Ag nanofluid are lower due to the rising of the nanoparticle volume fraction ϕ_2. The influences of the nanoparticle volume fraction ϕ_3 on the skin friction coefficients C_x and C_y of the Cu nanofluid are explained in Figures 25 and 26. The decreasing behavior in the skin friction coefficients C_x and C_y of the copper nanofluid is observed for expanding values of the nanoparticle volume fraction ϕ_3. Figure 27 analyzes the effect of the Schmidt

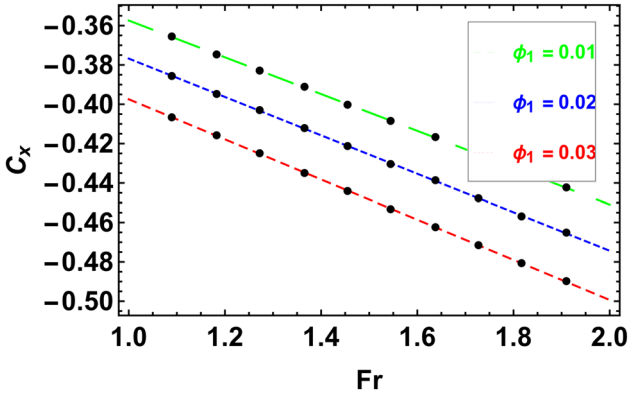

Figure 21: Variation in C_x *via* Fr for ϕ_1.

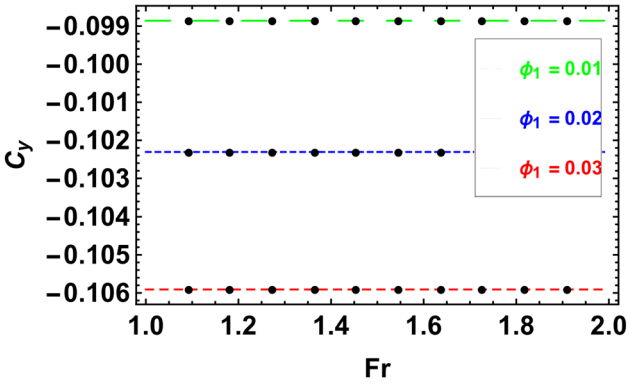

Figure 22: Variation in C_y *via* Fr for ϕ_1.

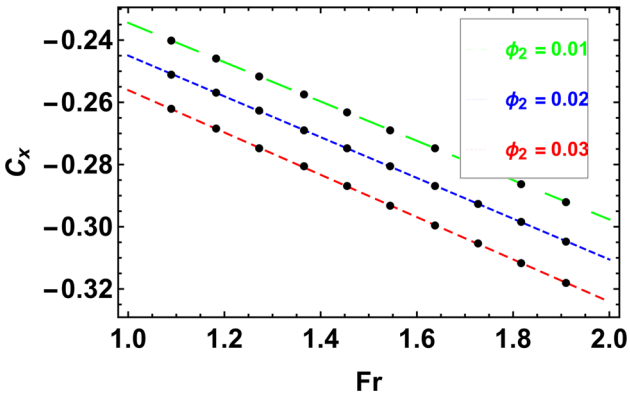

Figure 23: Variation in C_x *via* Fr for ϕ_2.

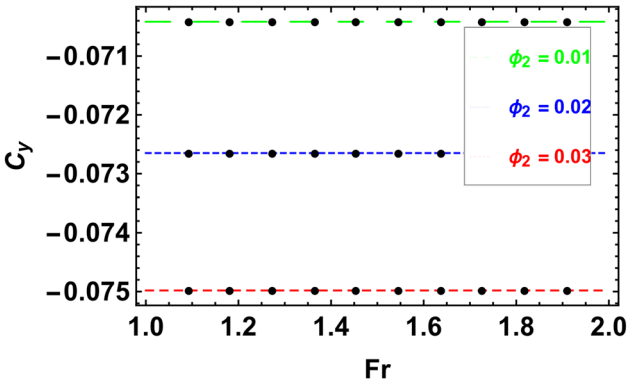

Figure 24: Variation in C_y *via* Fr for ϕ_2.

number Sc on the Sherwood number Sh of the ternary hybrid nanofluid *via* chemical reaction parameter kr. The decrement reaction of Sherwood number Sh of the ternary hybrid nanofluid is examined for rising estimation of the Schmidt number Sc *via* chemical reaction parameter kr.

The skin friction coefficients along x- and y-directions, Nusselt number, and Sherwood number against

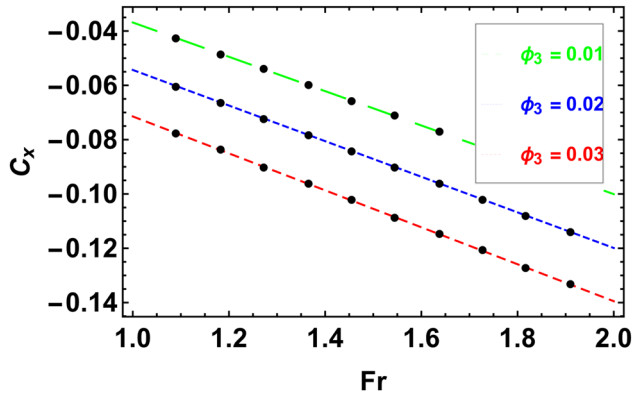

Figure 25: Variation in C_x *via* Fr for ϕ_3.

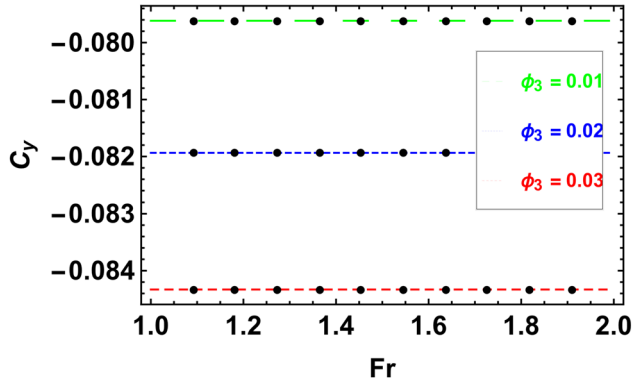

Figure 26: Variation in C_y *via* Fr for ϕ_2.

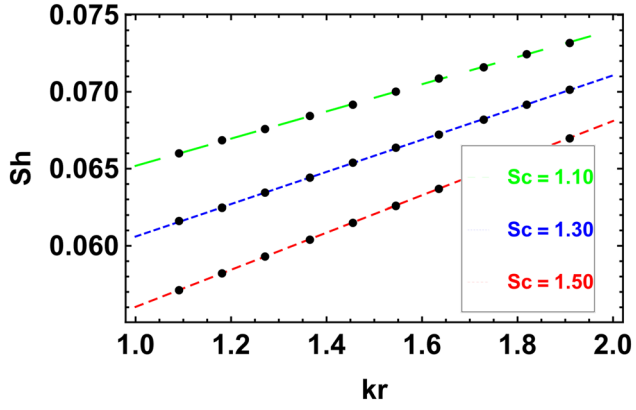

Figure 27: Variation in Sh *via* kr and Sc.

distinct flow parameters are also displayed in a tabular form. Table 2 presents the effect of nanoparticle volume fraction ϕ_{GO} nanoparticle volume fraction ϕ_{Ag}, and nanoparticle volume fraction ϕ_{Cu} on the skin friction coefficient C_x of the GO/kerosene oil nanofluid, Ag/kerosene oil nanofluid, and Cu/kerosene oil nanofluid. From this

Table 2: Effects of ϕ_{GO}, ϕ_{Ag}, and ϕ_{Cu} on C_x

ϕ_{GO}	ϕ_{Ag}	ϕ_{Cu}	C_x		
			GO-kerosene oil nanofluid	Ag-kerosene oil nanofluid	Cu-kerosene oil nanofluid
0.01	0.0	0.0	−0.009101	—	—
0.02	0.0	0.0	−0.009084	—	—
0.03	0.0	0.0	−0.009048	—	—
0.04	0.0	0.0	−0.008991	—	—
0.0	0.01	0.0	—	−0.008584	—
0.0	0.02	0.0	—	−0.008006	—
0.0	0.03	0.0	—	−0.007362	—
0.0	0.04	0.0	—	−0.006645	—
0.0	0.0	0.01	—	—	−0.012430
0.0	0.0	0.02	—	—	−0.011349
0.0	0.0	0.03	—	—	−0.010980
0.0	0.0	0.04	—	—	−0.0090406

table, it is noted that the skin friction coefficient C_x of the GO/kerosene oil nanofluid, Ag/kerosene oil nanofluid, and Cu/kerosene oil nanofluid are higher for nanoparticle volume fraction ϕ_{GO}, nanoparticle volume fraction ϕ_{Ag}, and nanoparticle volume fraction ϕ_{Cu}. The variations in the skin friction coefficient C_y of the GO/kerosene oil nanofluid, Ag/kerosene oil nanofluid, and Cu/kerosene oil nanofluid for expanding values of nanoparticle volume fraction ϕ_{GO}, nanoparticle volume fraction ϕ_{Ag}, and nanoparticle volume fraction ϕ_{Cu} are demonstrated in Table 3. The enhancing estimation of the nanoparticle volume fraction ϕ_{GO}, nanoparticle volume fraction ϕ_{Ag}, and nanoparticle volume fraction ϕ_{Cu} reduces the skin friction

Table 3: Effects of ϕ_{GO}, ϕ_{Ag}, and ϕ_{Cu} on C_y

ϕ_{GO}	ϕ_{Ag}	ϕ_{Cu}	C_y		
			GO/kerosene oil nanofluid	Ag/kerosene oil nanofluid	Cu/kerosene oil nanofluid
0.01	0.0	0.0	−0.033835	—	—
0.02	0.0	0.0	−0.034690	—	—
0.03	0.0	0.0	−0.035574	—	—
0.04	0.0	0.0	−0.036491	—	—
0.0	0.01	0.0	—	−0.033840	—
0.0	0.02	0.0	—	−0.034700	—
0.0	0.03	0.0	—	−0.035591	—
0.0	0.04	0.0	—	−0.036515	—
0.0	0.0	0.01	—	—	−0.033810
0.0	0.0	0.02	—	—	−0.034640
0.0	0.0	0.03	—	—	−0.035499
0.0	0.0	0.04	—	—	−0.036389

coefficient C_y of the GO/kerosene oil nanofluid, Ag/kerosene oil nanofluid, and Cu/kerosene oil nanofluid. Table 4 is drawn to evaluate the effect of nanoparticle volume fractions $\phi_{GO-Ag-Cu}$ over the skin friction coefficients C_x and C_y of the ternary hybrid nanoliquid. From this analysis, the enhancement in both skin friction coefficients C_x and C_y of the ternary hybrid nanoliquid is observed for intensifying values of the nanoparticle volume fractions $\phi_{GO-Ag-Cu}$. The numerical computation of the skin friction coefficients C_x and C_y *versus* expanding values of porosity parameter ε, rotating parameter Ω, ion-slip number γ_i, Hall current parameter γ_e, and magnetic parameter M is explained in Table 5. In this inquiry, it is scrutinized that escalating estimation of porosity parameter ε, rotating parameter Ω, and magnetic parameter M has increased the skin friction coefficient C_x, while the ion-slip number γ_i and Hall current parameter γ_e have declined the skin friction coefficient C_x. Also, it is detected that the intensification in porosity parameter ε, rotating parameter Ω, and magnetic parameter M raised the skin friction coefficient C_y of the ternary hybrid nanoliquid, while the skin friction coefficient C_y of the ternary hybrid nanoliquid is lower for ion-slip number γ_i and Hall current parameter γ_e The variations in Nusselt number Nu of the GO/kerosene oil nanofluid and Ag/kerosene oil nanofluid and Cu/kerosene oil nanofluid for nanoparticle volume fraction ϕ_{GO}, nanoparticle volume fraction ϕ_{Ag}, and nanoparticle volume fraction ϕ_{Cu} are discussed in Table 6. It is clear that the intensifying estimation of the nanoparticle volume fraction ϕ_{GO}, nanoparticle volume fraction ϕ_{Ag}, and nanoparticle volume fraction ϕ_{Cu} has elevated the Nusselt number Nu of the GO/kerosene oil nanofluid, Ag/kerosene oil nanofluid, and Cu/kerosene oil nanofluid. The behavior of the nanoparticles volume fractions $\phi_{GO-Ag-Cu}$ on ternary hybrid nanofluid on the Nusselt number Nu is displayed in Table 7. The augmentation in the Nusselt number Nu of the ternary hybrid nanoliquid is noticed for escalating estimation of the nanoparticles volume fractions $\phi_{GO-Ag-Cu}$. In view of the physical meaning, it is indicated that the thermal conductivity of the liquid is increased due to the increase in the nanoparticles volume fraction; therefore, the Nusselt

Table 4: Effect of $\phi_{GO-Ag-Cu}$ on C_x and C_y

$\phi_{GO-Ag-Cu}$	C_x	C_y
0.01	−0.012268	−0.035538
0.02	−0.011424	−0.033338
0.03	−0.010696	−0.034450
0.04	−0.009195	−0.032918

Table 5: Effects of ε, Ω, γ_i, γ_e, and M on C_x and C_y

ε	Ω	γ_i	γ_e	M	C_x	C_y
0.1	0.5	0.1	0.1	0.3	−0.220804	−0.264263
0.2	0.5	0.1	0.1	0.3	−0.218707	−0.261267
0.3	0.5	0.1	0.1	0.3	−0.216610	−0.259269
0.4	0.5	0.1	0.1	0.3	−0.204512	−0.255273
0.1	0.5	0.1	0.1	0.3	−0.220804	−0.264273
0.1	1.0	0.1	0.1	0.3	−0.219804	−0.261677
0.1	1.5	0.1	0.1	0.3	−0.216804	−0.258081
0.1	2.0	0.1	0.1	0.3	−0.215804	−0.252485
0.1	0.5	1.0	0.1	0.3	−1.232672	1.122613
0.1	0.5	1.5	0.1	0.3	−1.242827	1.013206
0.1	0.5	2.0	0.1	0.3	−1.302960	0.838007
0.1	0.5	2.5	0.1	0.3	−1.499713	0.678173
0.1	0.5	0.1	0.2	0.3	−2.168960	−0.073916
0.1	0.5	0.1	0.3	0.3	−2.174134	−0.078807
0.1	0.5	0.1	0.4	0.3	−2.189772	−0.083559
0.1	0.5	0.1	0.5	0.3	−2.205861	−0.088178
0.1	0.5	0.1	0.1	0.1	−0.320805	−0.264273
0.1	0.5	0.1	0.1	0.2	−0.318624	−0.199143
0.1	0.5	0.1	0.1	0.3	−0.286443	−0.134012
0.1	0.5	0.1	0.1	0.4	−0.274263	−0.068881

Table 6: Effects of ϕ_{GO}, ϕ_{Ag}, and ϕ_{Cu} on Nu

ϕ_{GO}	ϕ_{Ag}	ϕ_{Cu}	Nu		
			GO/ kerosene oil nanofluid	Ag/kerosene oil nanofluid	Cu/kerosene oil nanofluid
0.01	0.0	0.0	0.194663	—	—
0.02	0.0	0.0	0.566531	—	—
0.03	0.0	0.0	0.666086	—	—
0.04	0.0	0.0	0.674261	—	—
0.0	0.01	0.0	—	0.188918	—
0.0	0.02	0.0	—	0.536182	—
0.0	0.03	0.0	—	0.574411	—
0.0	0.04	0.0	—	0.613198	—
0.0	0.0	0.01	—	—	0.188968
0.0	0.0	0.02	—	—	0.536142
0.0	0.0	0.03	—	—	0.624353
0.0	0.0	0.04	—	—	0.713122

Table 7: Effect of $\phi_{GO-Ag-Cu}$ on Nu

$\phi_{GO-Ag-Cu}$	Nu
0.01	0.210584
0.02	0.566157
0.03	0.776797
0.04	0.892438

numbers of the nanofluid, hybrid nanofluid, and ternary hybrid nanoliquid are boosted. Further it can be detected that at $\phi_{GO} = 0.01$ and $\phi_{GO-Ag-Cu} = 0.01$, the Nusselt number of the ternary hybrid nanoliquid is augmented by 8%. At $\phi_{GO} = 0.04$ and $\phi_{GO-Ag-Cu} = 0.04$, the Nusselt number of the ternary hybrid nanofluid is amplified by 32%. At $\phi_{Ag} = 0.01$ and $\phi_{GO-Ag-Cu} = 0.01$, the Nusselt number of the ternary hybrid nanofluid is improved by 11%. At $\phi_{Ag} = 0.04$ and $\phi_{GO-Ag-Cu} = 0.04$, the Nusselt number of the ternary hybrid nanofluid is elevated by 46%. At $\phi_{Cu} = 0.01$ and $\phi_{GO-Ag-Cu} = 0.01$, the Nusselt number of the ternary hybrid nanofluid is enlarged by 11%. At $\phi_{Cu} = 0.04$ and $\phi_{GO-Ag-Cu} = 0.04$, the Nusselt number of the ternary hybrid nanoliquid is boosted by 25%. From the computation of the abovementioned numerical percentage, it is clear that by expanding the nanoparticle volume fraction, the thermal conductivities of the nanofluid, hybrid nanoliquid, and ternary hybrid nanoliquid are enlarged and the Nusselt numbers of the nanofluid, hybrid nanoliquid, and ternary hybrid nanoliquid are elevated. The impacts of ion-slip number γ_i, Hall current γ_e, Eckert number Ec, and magnetic parameter M on the Nusselt number Nu of the ternary hybrid nanofluid are displayed in Table 8. From this table, it is inspected that the ternary hybrid nanofluid Nusselt number Nu is higher for increasing values of the ion-slip number γ_i, Hall current γ_e, Eckert number Ec and magnetic parameter M. The aspect of the nanoparticle volume fraction ϕ_{GO}, nanoparticle volume fraction ϕ_{Ag}, and nanoparticle volume fraction ϕ_{Cu} on the Sherwood number Sh of the GO/kerosene oil nanofluid, Ag/kerosene oil nanofluid, and Cu/kerosene oil nanofluid are analyzed in Table 9. The increments in the Sherwood number Sh of the GO/kerosene oil nanofluid, Ag/kerosene oil nanofluid, and Cu/kerosene oil nanofluid are investigated due to the larger values of nanoparticle volume fraction ϕ_{GO}, nanoparticle volume fraction ϕ_{Ag}, and nanoparticle volume fraction ϕ_{Cu}. The deviation in the Sherwood number Sh of the ternary hybrid nanofluid against nanoparticles volume fractions $\phi_{GO-Ag-Cu}$ is inspected in Table 10. In this inspection, it is perceived that the ternary hybrid nanofluid Sherwood number Sh is improved due to the rising values of nanoparticle volume fractions $\phi_{GO-Ag-Cu}$. Table 11 enlightens the impact of activation energy E, Schmidt number Sc, chemical reaction parameter kr, and temperature difference parameter δ on the Sherwood number Sh of the ternary hybrid nanofluid. The decrement performance in the Sherwood number Sh of the ternary hybrid nanoliquid is examined for larger values of activation energy E, Schmidt number Sc, chemical reaction parameter kr, and temperature difference parameter δ.

Table 8: Effects of γ_i, γ_e, Ec, and M on Nu

γ_i	γ_e	Ec	M	Nu
1.0	0.1	0.3	0.1	0.852219
1.5	0.1	0.3	0.1	0.870754
2.0	0.1	0.3	0.1	0.884226
2.5	0.1	0.3	0.1	0.890434
0.1	0.2	0.3	0.1	0.889218
0.1	0.3	0.3	0.1	0.902486
0.1	0.4	0.3	0.1	0.904523
0.1	0.5	0.3	0.1	0.906588
0.1	0.1	0.1	0.1	0.964238
0.1	0.1	0.3	0.1	1.010009
0.1	0.1	0.5	0.1	1.115522
0.1	0.1	0.7	0.1	1.221035
0.1	0.1	0.3	0.1	0.724670
0.1	0.1	0.3	0.2	0.878117
0.1	0.1	0.3	0.3	0.891306
0.1	0.1	0.3	0.4	0.904496

Table 9: Effects of ϕ_{GO}, ϕ_{Ag}, and ϕ_{Cu} on Sh

ϕ_{GO}	ϕ_{Ag}	ϕ_{Cu}	Sh		
			GO/ kerosene oil nanofluid	Ag/kerosene oil nanofluid	Cu/kerosene oil nanofluid
0.01	0.0	0.0	0.090522	—	—
0.02	0.0	0.0	0.090544	—	—
0.03	0.0	0.0	0.090572	—	—
0.04	0.0	0.0	0.090573	—	—
0.0	0.01	0.0	—	0.090574	—
0.0	0.02	0.0	—	0.090576	—
0.0	0.03	0.0	—	0.090578	—
0.0	0.04	0.0	—	0.090580	—
0.0	0.0	0.01	—	—	0.090544
0.0	0.0	0.02	—	—	0.090562
0.0	0.0	0.03	—	—	0.090572
0.0	0.0	0.04	—	—	0.090582

Table 10: Effect of $\phi_{GO-Ag-Cu}$ on Sh

$\phi_{GO-Ag-Cu}$	Sh
0.01	0.090571
0.02	0.090573
0.03	0.090574
0.04	0.090575

Table 11: Effects of E, Sc, kr, and δ on Sh

E	Sc	kr	δ	Sh
0.2	0.1	0.1	0.1	0.090798
0.4	0.1	0.1	0.1	0.090589
0.6	0.1	0.1	0.1	0.090494
0.8	0.1	0.1	0.1	0.090399
0.1	0.3	0.1	0.1	0.090565
0.1	0.5	0.1	0.1	0.090363
0.1	0.7	0.1	0.1	0.090254
0.1	0.9	0.1	0.1	0.090146
0.1	0.1	0.4	0.1	0.090678
0.1	0.1	0.5	0.1	0.090415
0.1	0.1	0.6	0.1	0.090374
0.1	0.1	0.7	0.1	0.090333
0.1	0.1	0.1	0.5	0.090805
0.1	0.1	0.1	0.6	0.090804
0.1	0.1	0.1	0.7	0.090581
0.1	0.1	0.1	0.8	0.090580

7 Conclusion

In this investigation, the three-dimensional flow of ternary hybrid nanoliquid with magnetic field and Hall current effects through a rotating surface is explored. The influence of Darcy–Forchheimer, chemical reaction, and activation energy is also analyzed in the current examination. The heat and mass transport mechanisms are computed with the implementation of convective conditions. For the analytical simulation of the present problem, the homotopic analysis procedure is exploited. Some significant findings of the present study are listed as:

- Increasing trend in the skin friction coefficients C_x and C_y of the ternary hybrid nanofluid is noted *via* augmenting nanoparticle volume fraction ($\phi_{\text{GO–Ag–Cu}}$).
- The Nusselt number of the nanofluid and ternary hybrid nanofluid is augmented due to the increment of nanoparticle volume fraction. Further it can be perceived that at $\phi_{\text{GO}} = 0.01$ and $\phi_{\text{GO–Ag–Cu}} = 0.01$, the Nusselt number of the ternary hybrid nanofluid is augmented by 8%. At $\phi_{\text{GO}} = 0.04$ and $\phi_{\text{GO–Ag–Cu}} = 0.04$, the Nusselt number of the ternary hybrid nanofluid is amplified by 32%. At $\phi_{\text{Ag}} = 0.01$ and $\phi_{\text{GO–Ag–Cu}} = 0.01$, the Nusselt number of the ternary hybrid nanofluid is improved by 11%. At $\phi_{\text{Ag}} = 0.04$ and $\phi_{\text{GO–Ag–Cu}} = 0.04$, the Nusselt number of the ternary hybrid nanofluid is increased by 46%. At $\phi_{\text{Cu}} = 0.01$ and $\phi_{\text{GO–Ag–Cu}} = 0.01$, the Nusselt number of the ternary hybrid nanofluid is enlarged by 11%. At $\phi_{\text{Cu}} = 0.04$ and $\phi_{\text{GO–Ag–Cu}} = 0.04$, the Nusselt number of the ternary hybrid nanofluid is boosted by 25%.
- The Sherwood numbers of the nanofluid and ternary hybrid nanoliquid are higher when the nanoparticles volume fraction is higher.
- Along the primary direction, the augmentation in ternary hybrid nanoliquid velocity is noted due to the increment in Hall current and ion-slip number, while a reverse trend is observed *via* porosity parameter, Darcy–Forchheimer parameter, and magnetic field parameter.
- The higher values of Hall current and magnetic parameter led to enhance the secondary velocity of the ternary hybrid nanoliquid, while the secondary velocity was reduced due to the increase in the ion-slip number and rotation parameter.
- The temperature of the ternary hybrid nanoliquid is heightened for a thermal Biot number, Eckert number, and magnetic parameter, while the enhancing values of the Hall current and ion-slip number reduce the ternary hybrid nanoliquid temperature.
- The ternary hybrid nanoliquid concentration becomes lower for temperature difference parameter, chemical reaction parameter, and Schmidt number, while the activation energy diminishes the concentration of the ternary hybrid nanofluid.

Funding information: This research was funded by National Science, Research and Innovation Fund (NSRF), and King Mongkut's University of Technology North Bangkok with Contract no. KMUTNB-FF-65-24.

Author contributions: All authors have accepted responsibility for the entire content of this manuscript and approved its submission.

Conflict of interest: The authors have no conflict of interest.

References

[1] Farooq U, Waqas H, Imran M, Albakri A, Muhammad T. Numerical investigation for melting heat transport of nanofluids due to stretching surface with Cattaneo-Christov thermal model. Alex Eng J. 2022;61(9):6635–44.

[2] Li YX, Mishra SR, Pattnaik PK, Baag S, Li YM, Ijaz Khan M, et al. Numerical treatment of time dependent magnetohydrodynamic nanofluid flow of mass and heat transport subject to chemical reaction and heat source. Alex Eng J. 2022;61(3):2484–91.

[3] Sunthrayuth P, Abdelmohsen SAM, Rekha MB, Raghunatha KR, Abdelbacki AMM, Gorji MR, et al. Impact of nanoparticle

aggregation on heat transfer phenomena of second-grade nanofluid flow over melting surface subject to homogeneous-heterogeneous reactions. Case Stud Therm Eng. 2022;32:101897.
[4] Ramzan M, Khan NS, Kumam P. Mechanical analysis of non-Newtonian nanofluid past a thin needle with dipole effect and entropic characteristics. Sci Rep. 2021;11(1):1–25.
[5] Ramzan M, Khan NS, Kumam P, Khan R. A numerical study of chemical reaction in a nanofluid flow due to rotating disk in the presence of magnetic field. Sci Rep. 2021;11(1):1–24.
[6] Gul T, Rahman JU, Bilal M, Saeed A, Alghamdi W, Mukhtar S, et al. Viscous dissipated hybrid nanoliquid flow with Darcy–Forchheimer and forced convection over a moving thin needle. AIP Adv. 2020;10(10):105308.
[7] Ramzan M, Algehyne EA, Saeed A, Dawar A, Kumam P, Watthayu W. Homotopic simulation for heat transport phenomenon of the Burgers nanofluids flow over a stretching cylinder with thermal convective and zero mass flux conditions. Nanotechnol Rev. 2022;11(1):1437–49.
[8] Alghamdi M, Wakif A, Thumma T, Khan U, Baleanu D, Rasool G. Significance of variability in magnetic field strength and heat source on the radiative-convective motion of sodium alginate-based nanofluid within a Darcy-Brinkman porous structure bounded vertically by an irregular slender surface. Case Stud Therm Eng. 2021;28:101428.
[9] Rasool G, Wakif A. Numerical spectral examination of EMHD mixed convective flow of second-grade nanofluid towards a vertical Riga plate using an advanced version of the revised Buongiorno's nanofluid model. J Therm Anal Calorim. 2021;143(3):2379–93.
[10] Ashraf MU, Qasim M, Wakif A, Afridi MI, Animasaun IL. A generalized differential quadrature algorithm for simulating magnetohydrodynamic peristaltic flow of blood-based nanofluid containing magnetite nanoparticles: a physiological application. Numer Methods Partial Differ Equ. 2022;38(3):666–92.
[11] Mjankwi MA, Masanja VG, Mureithi EW, James MNO. Unsteady MHD flow of nanofluid with variable properties over a stretching sheet in the presence of thermal radiation and chemical reaction. Int J Math Sci. 2019;2019:7392459.
[12] Wakif A, Chamkha A, Animasaun IL, Zaydan M, Waqas H, Sehaqui R. Novel physical insights into the thermodynamic irreversibilities within dissipative EMHD fluid flows past over a moving horizontal Riga plate in the coexistence of wall suction and Joule heating effects: a comprehensive numerical investigation. Arab J Sci Eng. 2020;45(11):9423–38.
[13] Dawar A, Wakif A, Thumma T, Shah NA. Towards a new MHD non-homogeneous convective nanofluid flow model for simulating a rotating inclined thin layer of sodium alginate-based Iron oxide exposed to incident solar energy. Int Commun Heat Mass Transf. 2022;130:105800.
[14] Sabu AS, Wakif A, Areekara S, Mathew A, Shah NA. Significance of nanoparticles' shape and thermo-hydrodynamic slip constraints on MHD alumina-water nanoliquid flows over a rotating heated disk: The passive control approach. Int Commun Heat Mass Transf. 2021;129:105711.
[15] Ramzan M, Saeed A, Kumam P, Ahmad Z, Junaid MS, Khan D. Influences of Soret and Dufour numbers on mixed convective and chemically reactive Casson fluids flow towards an inclined flat plate. Heat Transf. 2022;51:4393–433.
[16] Khan U, Zaib A, Sheikholeslami M, Wakif A, Baleanu D. Mixed convective radiative flow through a slender revolution bodies containing molybdenum-disulfide graphene oxide along with generalized hybrid nanoparticles in porous media. Cryst. 2020;10(9):771.
[17] Khan MS, Mei S, Fernandez-Gamiz U, Noeiaghdam S, Khan A. Numerical simulation of a time-dependent electroviscous and hybrid nanofluid with Darcy-Forchheimer effect between squeezing plates. Nanomater. 2022;12(5):876.
[18] Gumber P, Yaseen M, Rawat SK, Kumar M. Heat transfer in micropolar hybrid nanofluid flow past a vertical plate in the presence of thermal radiation and suction/injection effects. Partial Differ Equ Appl Meth. 2022;5:100240.
[19] Ramzan M, Dawar A, Saeed A, Kumam P, Watthayu W, Kumam W. Heat transfer analysis of the mixed convective flow of magnetohydrodynamic hybrid nanofluid past a stretching sheet with velocity and thermal slip conditions. PLoS One. 2021;16(12):e0260854.
[20] Raja MAZ, Shoaib M, Khan Z, Zuhra S, Saleel CA, Nisar KS, et al. Supervised neural networks learning algorithm for three dimensional hybrid nanofluid flow with radiative heat and mass fluxes. Ain Shams Eng J. 2022;13(2):101573.
[21] Alsaedi A, Muhammad K, Hayat T. Numerical study of MHD hybrid nanofluid flow between two coaxial cylinders. Alex Eng J. 2022;61(11):8355–62.
[22] Khashi'ie NS, Arifin NM, Pop I. Magnetohydrodynamics (MHD) boundary layer flow of hybrid nanofluid over a moving plate with Joule heating. Alex Eng J. 2022;61(3):1938–45.
[23] Khan U, Zaib A, Ishak A, Sherif ES, Waini I, Chu YM, et al. Radiative mixed convective flow induced by hybrid nanofluid over a porous vertical cylinder in a porous media with irregular heat sink/source. Case Study. Therm Eng. 2022;30:101711.
[24] Khan U, Mahmood Z. MHD stagnation point flow of ternary hybrid nanofluid flow over a stretching/shrinking cylinder with suction and ohmic heating; 2022.
[25] Manjunatha S, Puneeth V, Gireesha BJ, Chamkha A. Theoretical study of convective heat transfer in ternary nanofluid flowing past a stretching sheet. J Appl Comput Mech. 2021.
[26] Animasaun IL, Yook SJ, Muhammad T, Mathew A. Dynamics of ternary-hybrid nanofluid subject to magnetic flux density and heat source or sink on a convectively heated surface. Surf Interfaces. 2022;28:101654.
[27] Algehyne EA, El-Zahar ER, Sohail M, Nazir U, AL-bonsrulah HA, Veeman D, et al. Thermal Improvement in Pseudo-Plastic Material Using Ternary Hybrid Nanoparticles *via* Non-Fourier's Law over Porous Heated Surface. Energ. 2021;14(23):8115.
[28] Elnaqeeb T, Animasaun IL, Shah NA. Ternary-hybrid nanofluids: significance of suction and dual-stretching on three-dimensional flow of water conveying nanoparticles with various shapes and densities. Z Naturforsch A. 2021;6(3):231–43.
[29] Raja MA, Shoaib M, Hussain S, Nisar KS, Islam S. Computational intelligence of Levenberg-Marquardt backpropagation neural networks to study thermal radiation and Hall effects on boundary layer flow past a stretching sheet. Int Commun Heat Mass Transf. 2022;130:105799.
[30] Das M, Nandi S, Kumbhakar B. Hall effect on unsteady MHD 3D Carreau nanofluid flow past a stretching sheet with Navier's slip and nonlinear thermal radiation. PJMs. 2022;11.
[31] Hussain SM, Jain J, Seth GS, Rashidi MM. Free convective heat transfer with Hall effects, heat absorption and chemical

reaction over an accelerated moving plate in a rotating system. J Magn Magn Mater. 2017;422:112–23.
[32] Rasheed HU, Islam S, Zeeshan W, Khan J, Abbas T. Numerical modeling of unsteady MHD flow of Casson fluid in a vertical surface with chemical reaction and Hall current. Adv Mech Eng. 2022;14(3):16878132221085429.
[33] Li P, Abbasi A, El-Zahar ER, Farooq W, Hussain Z, Khan SU, et al. Hall effects and viscous dissipation applications in peristaltic transport of Jeffrey nanofluid due to wave frame. Colloids Interface Sci Commun. 2022;47:100593.
[34] Khan A, Kumam W, Khan I, Saeed A, Gul T, Kumam P, et al. Chemically reactive nanofluid flow past a thin moving needle with viscous dissipation, magnetic effects and Hall current. PLoS One. 2021;16(4):e0249264.
[35] Khazayinejad M, Nourazar SS. Space-fractional heat transfer analysis of hybrid nanofluid along a permeable plate considering inclined magnetic field. Sci Rep. 2022;12(1):1–15.
[36] Arif M, Kumam P, Kumam W, Mostafa Z. Heat transfer analysis of radiator using different shaped nanoparticles water-based ternary hybrid nanofluid with applications: A fractional model. Case Stud Therm. 2022;31:101837.
[37] Rehman KU, Shatanawi W, Al-Mdallal QM. A comparative remark on heat transfer in thermally stratified MHD Jeffrey fluid flow with thermal radiations subject to cylindrical/plane surfaces. Case Stud Therm. 2022;32:101913.
[38] Rasheed HU, Khan W, Khan I, Alshammari N, Hamadneh N. Numerical computation of 3D Brownian motion of thin film nanofluid flow of convective heat transfer over a stretchable rotating surface. Sci Rep. 2022;12(1):1–14.
[39] Shoaib M, Raja MA, Farhat I, Shah Z, Kumam P, Islam S. Soft computing paradigm for Ferrofluid by exponentially stretched surface in the presence of magnetic dipole and heat transfer. Alex Eng J. 2022;61(2):1607–23.
[40] Arif M, Kumam P, Kumam W, Khan I, Ramzan M. A fractional model of Casson fluid with ramped wall temperature: engineering applications of engine oil. Comput Math Methods Med. 2021;3:e1162.
[41] Bejawada SG, Reddy YD, Jamshed W, Eid MR, Safdar R, Nisar KS, et al. 2D mixed convection non-Darcy model with radiation effect in a nanofluid over an inclined wavy surface. Alex Eng J. 2022;61(12):9965–76.
[42] Alkathiri AA, Jamshed W, Eid MR, Bouazizi ML. Galerkin finite element inspection of thermal distribution of renewable solar energy in presence of binary nanofluid in parabolic trough solar collector. Alex Eng J. 2022;61(12):11063–76.
[43] Eid MR, Mabood F. Entropy analysis of a hydromagnetic micropolar dusty carbon NTs-kerosene nanofluid with heat generation: Darcy–Forchheimer scheme. Therm Anal. 2021;143(3):2419–36.
[44] Parvin S, Isa S, Al-Duais FS, Hussain SM, Jamshed W, Safdar R, et al. The flow, thermal and mass properties of Soret-Dufour model of magnetized Maxwell nanofluid flow over a shrinkage inclined surface. PLoS One. 2022;17(4):e0267148.
[45] Jamshed W, Mohd Nasir NAA, Brahmia A, Nisar KS, Eid MR. Entropy analysis of radiative [MgZn6Zr-Cu/EO] Casson hybrid nanoliquid with variant thermal conductivity along a stretching surface: Implementing Keller box method. Proc Inst Mech Eng C J Mech Eng Sci. 2022;09544062211065696.
[46] Shahzad F, Bouslimi J, Gouadria S, Jamshed W, Eid MR, Safdar R, et al. Hydrogen energy storage optimization in solar-HVAC using Sutterby nanofluid *via* Koo-Kleinstreuer and Li (KKL) correlations model: A solar thermal application. Int J Hydrog Energy. 2022;47:18877–91.
[47] Safdar R, Gulzar I, Jawad M, Jamshed W, Shahzad F, Eid MR. Buoyancy force and Arrhenius energy impacts on Buongiorno electromagnetic nanofluid flow containing gyrotactic microorganism. Proc Inst Mech Eng C J Mech Eng Sci. 2022;09544062221095693.
[48] Shahzad F, Jamshed W, Devi SSU, Safdar R, Prakash M, Ibrahim RW, et al. Raising thermal efficiency of solar water-pump using Oldroyd-B nanofluids' flow: An optimal thermal application. Energy Sci Eng. 2022
[49] Khan M, Lone SA, Rasheed A, Alam MN. Computational simulation of Scott-Blair model to fractional hybrid nanofluid with Darcy medium. Int Commun Heat Mass Transf. 2022;130:105784.
[50] Shafiq A, Lone SA, Sindhu TN, Al-Mdallal QM, Rasool G. Statistical modeling for bioconvective tangent hyperbolic nanofluid towards stretching surface with zero mass flux condition. Sci Rep. 2021;11(1):1–11.